NASA CONTRACTOR REPORT

NASA CR-1992

EFFECT OF METALLURGICAL STRUCTURE AND PROPERTIES ON ADHESION AND FRICTION BEHAVIOR OF COBALT ALLOYS

by D. V. Keller, Jr., S. Shatynski, and P. M. Vedamanikam

Prepared by
SYRACUSE UNIVERSITY
Syracuse, N.Y. 13210
for Lewis Research Center

NATIONAL AERONAUTICS AND SPACE ADMINISTRATION • WASHINGTON, D. C. • MARCH 1972

1. Report No.	2. Government Accession No.	3. Recipient's Catalog No.
NASA CR-1992		

4. Title and Subtitle: EFFECT OF METALLURGICAL STRUCTURE AND PROPERTIES ON ADHESION AND FRICTION BEHAVIOR OF COBALT ALLOYS

5. Report Date: March 1972

6. Performing Organization Code:

7. Author(s): D. V. Keller, Jr., S. Shatynski, and P. M. Vedamanikam

8. Performing Organization Report No.: None

10. Work Unit No.:

9. Performing Organization Name and Address:
Syracuse University
Syracuse, New York 13210

11. Contract or Grant No.: NGL-33-022-108

13. Type of Report and Period Covered: Contractor Report

12. Sponsoring Agency Name and Address:
National Aeronautics and Space Administration
Washington, D.C. 20546

14. Sponsoring Agency Code:

15. Supplementary Notes:
Project Manager, Robert L. Johnson, Fluid System Components Division, NASA Lewis Research Center, Cleveland, Ohio

16. Abstract

The metallurgical structure and some of the mechanical properties (hardness, strength, etc.) of two cobalt alloys, cobalt-50% iron and cobalt-25% molybdenum-10% chromium, were determined under various heat treated conditions. The mechanical properties of the bcc disordered Co-50Fe alloy, which was found to be very brittle, indicated an exceedingly low fracture strength, low hardness, and very weak grain boundary strength. Ordering by suitable heat treatment only produced a more brittle material with a lower fracture strength and a slightly higher hardness value. Work hardening was found to produce a finer grain structure and a greater grain boundary strength. The composite structured Co-25Mo-10Cr in the as-cast condition had a hardness value of Rockwell C-49 and was quite susceptible to microcracking from thermal stresses. The tensile properties were examined. It was found that the Co-25Mo-10Cr alloy was difficult to place in the α-Co solid solution condition, which limited the ability to use precipitation as a hardening reaction. Over two hundred adhesion cycles from zero contact load, to maximum load, to fracture were conducted between couples for each of the above alloys in an ultrahigh vacuum system which would permit the sample surfaces to be cleaned of all contaminant layers. In the Co-50Fe case, the calculated fracture stress from the adhesion tests showed values in the range of 80 to 150 k.s.i. (in some cases even much higher values), which is about ten times greater than the values from tension tests. The contact behavior gave lower than anticipated adhesion strength for a bcc alloy and hence a lower friction coefficient, but a higher value relative

17. Key Words (Suggested by Author(s)):
Adhesion
Friction
Cobalt alloys
Structure
Mechanical properties

18. Distribution Statement:
Unclassified - unlimited

19. Security Classif. (of this report)	20. Security Classif. (of this page)	21. No. of Pages	22. Price*
Unclassified	Unclassified	118	$3.00

* For sale by the National Technical Information Service, Springfield, Virginia 22151

1. Cobalt alloys - Metallurgy -
2. Metallurgy -
3. Adhesion -
4. Friction tests -

to the Co-25Mo-10Cr alloy. On the other hand, the Co-25Mo-10Cr alloy had a fracture strength, from adhesion tests, around 180 k.s.i., or about five times the value from tension tests. The fracture mode of the adhesion junction was much like that of Co-50Fe, i.e., it appeared to be ductile. On the basis of contact behavior, the alloy was found to be a good bearing alloy. The most significant contribution of this study is the increased evidence that dynamic coefficient of friction values can be reasonably predicted from static adhesion data.

TABLE OF CONTENTS

LIST OF FIGURES

LIST OF FIGURES (Cont.)

PAGE

FIGURE

LIST OF FIGURES (Cont.)

PAGE

FIGURE

LIST OF SYMBOLS

A	REAL CONTACT AREA
A_I	AREA OF CONTACT DERIVED FROM HOLM'S EQUATION
A_N	REAL CONTACT AREA BASED ON MULTIPLE CONTACTS
A_o	INITIAL CONTACT AREA ON LOADING
a	RADIUS OF TRUE CONTACT AREA
a_i	RADIUS OF i^{th} METAL CONTACT
C	TEMPERATURE DEPENDENT CONSTANT
E	ELASTIC MODULUS
F	FRICTIONAL FORCE
F_t	FORCE EXPERIENCED BY THE INTERFACE SYSTEM
H	HARDNESS
i	CURRENT
m	TEMPERATURE INDEPENDENT CONSTANT
n	NUMBER OF CONTACTS
R_o	OBSERVED CONTACT RESISTANCE
R_o^o	CONTACT RESISTANCE AT ZERO LOAD
R_c	CONSTRICTION RESISTANCE
R_f	FILM RESISTANCE
S_{ij}	DISTANCE BETWEEN THE i^{th} and j^{th} CONTACT
t	CONTACT TIME AT CONSTANT LOAD
w	LOAD
x	ARBITRARY CONSTANT

Y	YIELD STRENGTH
α	ADHESION COEFFICIENT (IN EQUATION 4)
α	A CONSTANT (IN EQUATION 20)
β	RADIUS OF CURVATURE OF PEAKS OF THE ASPERITIES
τ	MEAN SHEAR STRENGTH OF THE WEAKEST PLANE IN THE CONTACT AREA
δ	STANDARD DEVIATION OF THE ASPERITY HEIGHT DISTRIBUTION
ϕ	POTENTIAL DROP
ρ	BULK RESISTIVITY OF METAL
Ω	OHM
$m\Omega$	MILLIOHM
$\mu\Omega$	MICRO-OHM
σ	STRESS*
ε	STRAIN*
ψ	PLASTICITY INDEX
*	APPARENT STRESS-STRAIN; cf. DISCUSSION IN TEXT

INTRODUCTION

The purpose of this research investigation was to determine the specific relationships between metallurgical crystal structure, i.e. hardenability modes, etc. and the corresponding adhesion and friction behavior of two specific cobalt alloys: Co-50Fe and Co-25Mo-10Cr.

From a technological point of view, metallic adhesion plays an important role in all phenomena involving the physical contact of two surfaces, particularly in the fields of friction and wear. In addition, the study of metallic adhesion is expected to provide further information concerning the nature and properties of surfaces which in turn could expand our understanding of processes such as sintering, fretting, corrosion, metal forming operations etc.

Adhesion may be defined[1] as the establishment of quasi-equilibrium attractive forces between two bodies in or near physical contact. Bailey[2] investigated adhesion phenomena between cleaved mica surfaces which were chemically clean and molecularly flat. She found that the adhesion strength was virtually equal to the cohesive strength of the parent body. Tabor's results[3] with mica indicated that surface forces were very strong for distance of separation up to 5 - 10A^{o}, but diminished rapidly beyond this separation.

Metal surfaces prepared by common metallographic techniques are usually covered[4] with asperities (surface roughness) which are from 10 - 300μ ($1\mu = 10^{-3}$mm) in height and spaced from 50 - 300μ apart depending upon the care of preparation. Asperities may be regarded as a segment of

a sphere with an average slope of the sides ranging from 5 - 10°[4]. The normal height distribution of the asperities has been shown to be Guassian[4].

Frictional force (F) as described by the adhesion theory of friction[5] is generally accepted as the sum of forces required to shear adhesion junctions and force required to plow interlocking asperities. If the adhesion term and the deformation term are considered to act independently, Bowden[3] showed that the friction force can be expressed as:

$$F = A\tau + A'P \qquad (1)$$

where τ is the mean shear strength of the weakest planes at the contact areas, A is the total real contact area, A' is the area of interlocked asperities and P is the yield pressure.

In the recent years, considerable effort has been expended in the development of a detailed explanation of metallic adhesion and contact phenomena for static systems, on the basis that if the static phenomena were understood, one would be in a position to understand the dynamic process, i.e. friction, more clearly. Johnson and Keller[6] showed that the contaminant film was the major barrier to metallic adhesion and that the condition of bulk miscibility could not be considered as a criterion for adhesion. Greenwood and Williamson[7] asserted that contact between solids was controlled by a plastic index (Ψ) of the materials in contact. The term was related to two material constants, i.e. the elastic constant (E) and hardness (H) and two topographic properties, i.e. the radius of curvature of peaks of the asperities (β) and standard deviation of the

height distribution of the summit (δ). The plastic index was presented in mathematical form as:

$$\Psi = \frac{E}{H}\sqrt{\frac{\delta}{\beta}} \qquad (2)$$

Buckley showed that the adhesion strength of numerous metal couples was highly anisotropic e.g. cf. Copper[8], and that of other metal systems was structure dependent.[9] Conrad and Rice[10] studied the adhesion of polycrystalline copper with different levels of impurities and correlated the adhesion coefficients (α) of the various systems where the adhesion coefficient (α) is defined as the ratio of fracture load of the adhesion couple to the impressed load. Their results indicated a relationship:

$$\alpha\, E = \text{Constant} \qquad (3)$$

where E is the elastic constant of the contacting materials. Gilbreath[11] correlated the adhesion coefficient with contact time (t) at constant load through an expression:

$$\alpha = Ct^{m} \qquad (4)$$

where C is a temperature dependent constant and m is a temperature independent constant. Preliminary and exploratory experiments using field ion microscopy to study atomic details of the mechanism of adhesion was presented by Muller et al.[12]

Contact resistance measurements between crossed wire samples were shown to permit a rather fine degree of characterization of the contacting surfaces with regard to contaminants, surface roughness and the mechanical

properties of the substrate during loading[13]. The contact resistance technique as described by Keller and McNicholas[13] was employed in an investigation utilizing ultra pure iron couples in which the carbon concentration was less than 8 ppm. Keller and McNicholas showed that gross metallic adhesion was not a characteristic of the iron - 65 ppm carbon system due possibly to the presence of carbides which precipitated on the iron surfaces after an annealing (degassing) process. Iron with 8 ppm carbon was chosen to extend their investigation on the deformation, adhesion and fracture of asperity junctions formed between two iron surfaces in contact. Since the adhesion process provides a part of the resistance to tangential motion in a friction system, a further purpose of this research was to examine possible solid state mechanisms which would provide low shear strength contaminants to the interface system such that the adhesion process could be minimized, and in turn, reduce friction. Keller and Tsai[14] used hydrogen as a contaminant gas and investigated its effect on the adhesion of iron - 8 ppm carbon couples. They showed that hydrogen, unlike oxygen and carbon developed a conductive adsorbed film on an iron surface which exhibited plastic deformation during compressive contact. The hydrogen film did not act as a barrier to the adhesion of iron couples. Hydrogen ion$^{(+)}$ impingement, however, created a barrier to adhesion. It was also observed that large quantities of hydrogen were not found to dissolve in the iron.

The present investigation is a direct outgrowth of the previous research program which is more general in the sense that all material

properties are being investigated in conjunction with the metallic adhesion phenomena yet more specific in that two specifically selected materials (Co-50Fe and Co-25Mo-10Cr) are being considered in this light. The long range purpose of this present program is to develop metallurgical criteria for bearing alloys based on our knowledge of metal structure, adhesion behavior and friction behavior which was generated through the published works of Johnson and Keller et al.[6, 15, 17]. In effect, the principles of materials science are being brought to bear to provide better bearing systems rather than more or less arbritrarily choosing an alloy and then solving the friction problem through a choice of lubricant. For example, a research group[8, 9] at NASA Lewis Research Laboratories (Cleveland, Ohio) while working in ultra high vacuum friction investigations, identified certain hexagonal metal systems, e.g. cobalt, which demonstrate an abnormally low coefficient of friction relative to the other transition metals under severe conditions. Their research on these alloys, did not, however, attempt to uncover the optimum metallurgical heat treatment (sub-structure) for these particular alloys or an extensive correlation of these sub-structures with the friction or adhesion data. A qualitative relationship has been shown to exist[8, 9]; however, the development of complete correlation between these parameters will identify all of the variables and their importance, and establish guide lines for the identification of new bearing combinations.

THEORY

Metallic Adhesion Theory

Two metallic surfaces brought into physical contact are usually said to experience "metallic ahdesion" if an observable net tensile load is required to separate the joined system[15]. The magnitude of metallic adhesion is dependent on physical and chemical properties of metals, the nature and extent of loading and the characteristics of contaminant layers present on all but atomically clean surfaces. Keller[16] categorized the metallic adhesion analysis into four sub-groups: interfacial, solution, electronic and fracture, which are based on a particular model of the interacting system. At this time, no direct experiments have been conducted successfully to obtain the interfacial energy and/or force of interfacial attraction in metallic systems as expressed by the first three models. The fracture model[15] although not capable of providing force of attraction data on an absolute scale, does provide a realistic analysis of the system.

The model examines metallic adhesion, the resistance to tensile separation of the surfaces in contact, through a consideration of the critical fracture stress of the regions making up the real contact area. Due to surface roughness, each asperity contact point will have undergone, during the compression cycle, various degrees of deformation from elastic contact to nearly 100% plastic flow. The contaminant layers present on the contacting surfaces have, for the most part, a low critical fracture stress relative to the metal substrate; but these

layers can be dispersed effectively by energy inputs to the interface system. Effective dispersal of the contaminating layers, e.g. rendering these layers inactive in preventing metal-metal bonding, is effected by mechanical energy such as gross plastic deformation, vibration and/or thermal dispersal as discussed by Keller et al.[15] and illustrated by the works of Milner[16]. Since the critical fracture stress of a grain boundary is the upper bound of the adhesion junction strength, (for a system without an interfacial contaminant) and that a non-conducting sorbed gas fixes the lower bound, adhesion junction strengths therefore depend on the ability of the physical contact mechanics to disperse the contaminant layer which is present. If no contaminants are present, the stress on each asperity contact, the summation of applied and residual stresses must exceed a critical fracture stress (σ^c) which is approximately that of a grain boundary of the weaker material. Note, that the mechanical energy is unnecessary since dispersal of the contaminant barrier is not involved. Barrier dispersal, as shown by Milner[16], is a most complex process as it depends on the physical properties of the metal as well as the chemistry of the contaminant system.

The force (F_t) experienced by the interface system based on the above concepts can be presented as:

$$F_t = \sum_{ij}^{n} \sigma_i \, (K_{ij})_x \, W_{ij}^{\,x} \qquad (5)$$

where K must be evaluated under conditions of the deformation process involved in expanding the i^{th} asperity which establishes the power of

W, the load, σ_i is the effective stress developed on the i^{th} asperity junction and the total force represents the effects of n junctions. The path the crack will follow on unloading the system will be that of the least resistance, e.g. the chemical composition of the fracture surfaces will not be identical to those before contact since material transport is expected in all areas. In an implicit manner the model suggests that an absolute correlation of adhesion data with atomic properties, structure of material, or defect mechanics require a rather adventurous extrapolation, if any but the grossest of generalizations are involved.

Keller[17] established three criteria for metallic adhesion using contact resistance techniques

1. A load approaching the fracture strength of the weaker material is required to fracture the adhesion junction if no contaminants are present.

2. The minimum contact resistance observed at maximum load on the couple is constant with unloading to, or very near to, the point of junction failure.

3. The contact resistance values are stable even under extremely light loading.

Theories of Friction

Although the use of lubricants for the mitigation of friction and wear dates back to the Egyptian civilization[18], it was in the fifteenth century that the basic laws of friction were experimentally established

by Leonardo da Vinci. These are that the frictional force is proportional to load and that it is independent of the apparent area of contact. These observations which were ignored were rediscovered two centuries later by the French architect Amontons[19]. His work was confirmed by other investigators, and explanations based on surface roughness were offered, such as Coulomb's interlocking theory, none of which have wide support at this time[20]. The contribution of this early work on friction is the realization that actual physical contact occurs only at discrete points within the apparent area of contact, at those points where the surface asperities happen to touch, by chance.

Desaguliers, an English scientist, found strong adhesion between lead spheres which had been truncated and then pressed together with a twisting motion, and based on this observation, postulated that adhesion is a significant component of friction[21]. Some early investigators such as Coulomb and Vince, considered adhesion as contributing to the frictional force, but, contrary to the modern theory, concluded that it represented only a small factor[20, 22]. Also among those rejecting adhesion as a major component of friction was Leslie, who realized that energy required for asperity deformation may be a significant factor[23]. This represents what the modern frictional theory calls " a ploughing effect or plastic deformation[24]".

That an adhesive force represents a major factor conbributing to frictional force was recognized in more modern times by Ewing, Hardy and Tomlinson, although the nature of the adhesive force was not established

nor was its presence experimentally verified.[25, 26, 27]. Bowden and Tabor have refined the adhesion theory of friction, and their work and other supporting contributions are presented in two volumes[28, 29]. Braithwaite provides a concise discussion of the modern adhesion (or welding) theory of friction, including the various arguments against it and their defense[30]. Additionally, he reviews other current theories of friction representing different mechanisms which may be of consequence in some situations.

Thus the adhesion theory of friction has evolved, recognizing that when surfaces are in contact they actually touch on only a fraction of the apparent area of contact, and that adhesion and shearing in these areas of real contact between the bulk materials or surface films is responsible for the major portion of frictional force.

While the theory of friction teaches that the real area of contact and the properties of the materials in contact, including surface films, determine the frictional resistance to sliding, quantitative evaluation of frictional force is a complex problem. One principal aspect of such an analysis is the determination of the real area of contact.

Contact Resistance Theory

The observed contact resistance (R_o) which results from the measurement of contact resistance between two crossed wires in the configuration:

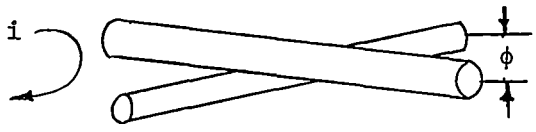

Figure 1

and measured as a potential drop (ϕ) when a current (i) is impressed across the system is given by:

$$R_o = R_c \pm R_f \tag{6}$$

where R_c is the pure constriction resistance which is a consequence of the current flow being constricted through small conducting spots (i.e.) the contact area) and R_f is resistance due to the contaminant film (+) or due to tunneling (-).

The film resistance may be assumed constant and negligible in the case of ultra clean metallic surfaces[15].

Holm[31] has shown that the constriction resistance of a single contact between similar metals is given by:

$$R_c = \frac{\rho}{2a} \tag{7}$$

where $\underline{a}$ is the contact radius of the true contact area and ρ is the bulk resistivity of metal.

Greenwood[32] explored the constriction resistance in a system of multiple contact points and showed that

$$R_c \simeq \frac{\rho}{2 \sum_i a_i} + \frac{\rho}{\pi n^2} \sum_i \sum_j \frac{1}{S_{ij}} \tag{8}$$

where: ρ = resistivity of bulk metal

a_i = radius of the i^{th} metal contact

n = number of contacts

S_{ij} = distance between the i^{th} and j^{th} contact

Greenwood[32] also provided the information which permitted the development by McNicholas, of an approximate relationship between the area of contact (A_I) derived from Holm's equation and real contact area (A_N) based on ($\underline{n}$) multiple contacts:

$$\frac{A_I}{A_N} \simeq 1.4\ n^{1/2} \tag{9}$$

where $n \simeq 30$[12]

Tabor[33] indicated that the area (A) observed in hardness studies could be related to the impressed load (W) and the yield strength (Y) by the equation:

$$A_N = \frac{W}{3Y} \tag{10}$$

Combining equations, 7, 9 and 10, we obtain a relationship between the observed contact resistance and load, which is given by:

$$\frac{A_I}{A_N} = 1.4n^{1/2} = \frac{\pi\ (\rho/2R_c)^2}{W/3Y} \tag{11}$$

or, by rearranging as:

$$R_c = 1.3n^{-1/4}\ Y^{1/2}\ \rho\ W^{-1/2} \tag{12}$$

The observed contact resistance versus load data can also be presented as an <u>apparent</u> stress-strain curve if suitable assumptions are made. The real area can be presented as:

$$A_N = \frac{A_I}{1.4n^{1/2}} = \frac{\pi\ (\rho/2\ R_c)^2}{1.4n^{1/2}} = 0.56\ \rho^2\ n^{-1/2}\ R_c^{-2} \tag{13}$$

Since stress (σ) in the system can be represented as:

$$\sigma = \frac{W}{A_N} \tag{14}$$

then by substituting equation (13) into equation (14) we obtain:

$$\sigma = 1.78\, n^{1/2}\, \rho^{-2}\, W\, R_c^{\,2} \tag{15}$$

Assuming that the system volume is constant, the apparent strain (ε) can be represented as:

$$\varepsilon = \ell n\, \left(\frac{A_o}{A}\right) \tag{16}$$

where A_o is the true area at initial contact as the load approaches zero and A is true area of contact at any other load.

By substituting equation (13) into equation (16), the strain (ε) is:

$$\varepsilon = 4.61 \log \left(\frac{R_o}{R_o^o}\right) \tag{17}$$

where R_o^o is the contact resistance at zero load and R_o is the contact resistance at any other load.

A direct substitution of the information obtained from the contact resistance - load curve will produce data for the apparent compressive stress and strain in the contacting system. A considerable degree of care must, however, be exercised in the interpretation of the data since the stresses and strains are not directly comparable to the common engineering terms. For example, as the load is increased the area expansion is due to deformation of the asperities as well as a geometric correction factor which must account for the apparent area increase caused by the shape of the

asperities. The latter term could be significant at extremely small loads. The initial area A_o is that area at initial contact as the load approaches zero; the strain, therefore is the measure of the expanding load bearing area from that point as the load is impressed (e.g. stress increased). Both terms are subject to the assumptions used in the development of the initial equation which was based on the research of Greenwood as well as the naivete of the stress analysis of this complex system. Since near zero load contact only involves the shape change of a few asperities, the change in system strain is expected to be quite large if these few asperities can collapse to a large degree in order to support the impressed load. In such a system, two conditions are immediately apparent: firstly, the elastic deformation of the first few asperities in the collapse process will probably not be observed since collapse will be almost instantaneous due to the relatively fast loading rate; secondly, the observed deformation is that of the asperities, a micro-process involving only a few microns square and does not reflect the changes in the macro-system, i.e. the bulk elastic limit for this system of contact will not have been achieved. The asperities will, therefore, collapse giving the appearance of a large degree of strain until sufficient asperities have been involved to incorporate a reaction due to the bulk dimensions of the system. A simple analogy can be drawn by placing one's foot on a grass lawn, the grass is severely strained before the load is supported in an elastic manner by the underlying earth. If the stress-strain diagram of this system is based on the area of contact which is involved (under foot) from the point of initial contact, the resulting strain relates directly to the collapse of the system under load. The asperity stress-strain system outline above can be regarded in a similar manner.

EXPERIMENTAL

Materials

Vacuum cast alloy plates (3/8" x 8" x 10") of the exact composition, Cobalt - 47.80 Iron* and Cobalt - 24.10 Molybdenum - 9.60 Chromium* were received from Materials Research Corporation. The alloys were prepared from high purity grade base metals such that the semiquantitative emission spectrographic analysis of each could be presented as:

	Element	Concentration Range
Co-50Fe Alloy	Si	0.0001 - 0.001%
	Pb, Cr, Al	0.001 - 0.01%
	Mg, Cu, Mo, Ni	0.01 - 0.10%
	Others	Not detected
Co-25Mo-10Cr Alloy	Si	0.0001 - 0.001%
	Pb, Zn	0.001 - 0.01%
	Mg, Al, Fe, Cu, Ni	0.01 - 0.1%
	Others	Not detected

Each alloy presented its own distinct problems in the reduction of the alloy plates into tensile, adhesion and x-ray specimens. The Co-50Fe alloy could be reduced to rectangular blocks either by hacksawing or cooled cut-off wheel techniques; however, tool machining was found to be almost impossible due to the very brittle nature of the alloy (c.f. discussion of tension test later). The necessary tool pressure to permit a cut in the lathe was sufficient to cause fracture of the sample, even though center support techniques were used. All specimens, as a consequence, were reduced

*All analytical values are in weight percent as supplied by Materials Research Corporation.

by wet grinding methods.

The Co-25Mo-10Cr alloy could only be reduced by careful cut-off wheel techniques since the alloy in the "as-cast" condition had a hardness value of Rockwell C-49 (R_c-49) and was quite susceptible to thermal cracking when the cut-off point was allowed to overheat due to improper cutting speed and/or cooling water flow. Machining of this alloy was barely possible with carbide tipped tools.

The tools used for investigating the metallurgical structure and properties of the alloys were x-ray diffraction and optical and electron microscopy. The tension tests were conducted on an Instron testing machine. Adhesion studies were done utilizing the techniques developed by Keller[13].

The structure of the Co-50Fe and Co-25Mo-10Cr alloys in the "as-cast" and other heat treated conditions were determined by x-ray diffraction techniques using Cr-Kα radiation and a vanadium filter. Hardness values of both alloys under various conditions were recorded.

Cobalt-50 Iron System

According to Ellis and Greiner[34], Hansen[35], Pearson[36] and others, alloys in the range of 50 w/o Co with a balance of Fe are subject to two polymorphic transformations:

$$\gamma \text{ (f.c.c.)} \underset{\leftarrow}{\overset{980^{\circ}C}{\rightleftharpoons}} \alpha \text{ (b.c.c. disordered)}$$

$$\alpha \text{ (b.c.c. disordered)} \underset{\leftarrow}{\overset{730^{\circ}C}{\rightleftharpoons}} \alpha \text{ (b.c.c. ordered)}$$

These principal solid state transformations occur for all alloys in the range of 50±20 w/o cobalt with some corrosponding decrease in transformation temperature as the cobalt concentration varies from about 50 w/o.

The literature[34, 35, 36] is not specific in regards to the kinetics of the ($\gamma \rightarrow \alpha$) transformation, although Ellis et al.[34] do mention that some thermal hystersis was observed in the thermal arrest data for the alloys in the range of 50 w/o Co. The existence of the γ(fcc) phase at room temperature has not been mentioned by any investigators which suggests that the transformation rate of the reaction ($\gamma \rightarrow \alpha$) on cooling is faster than the rate of cooling experienced by an alloy in the conventional "as-cast" plate. Whether or not the γ-phase can be retained by oil quenching techniques has not been verified.

The rate of transformation from the bcc-disordered phase to the bcc ordered phase (of the Cesium Chloride structure, B2 type) is exceedingly slow, so that all "as-cast" or air cooled samples are entirely of the disordered structure as are samples which were not exposed to extended heat treatment at temperatures between 700 - 730°C for at least 100 hours or the equivalent [34, 36]. Detailed kinetic data for this transformation are also lacking.

The structure of the "as-cast" Co-50Fe alloy was determined by x-ray diffraction techniques using filtered Cr radiation. Strong diffraction peaks were observed at (2θ) values of 68, 106 and 157 degrees which correspond to reflections of (hkl) indices (101), (200) and (211) respectively. This indicated a disordered body centered cubic structure with a unit cell dimension of about 2.85 A° which is consistent with literature[36]. No diffraction peaks were observed at 2θ values of 51, 88 and 126 degrees corresponding to reflections of (hkl) indices (100), (111) and (210) respectively which should have been present with the other lines if the structure were ordered. The lack of ordered bcc diffraction peaks in the "as-cast" samples is consistent with the observations of previous investigators[34, 35, 36].

The stress strain diagrams from four samples of the "as-cast" Co-Fe alloy were simple in that they both were very nearly straight lines to the

ultimate tensile strength (or fracture stress) in the range 9000 to 17000 psi, (Table 1) and a total strain of 5×10^{-4} inch/inch. The scatter in data was expected of a very brittle material with low grain boundary strength due to grain boundary porosity, evident in Figures 2 and 3. The fracture surfaces after the tension tests, were typical of brittle fractures with no reduction in cross section area. The tension tests were made with samples 0.296 inch diameter and a 1.00 inch test section on an Instron testing machine. The samples were very soft with a Rockwell hardness value of B-78 (average of nine tests with a very small scatter).

Two plates (3/8 x 4 x 4 inch) of the Co-Fe alloy were annealed for 60 hours at 1200°C in vacuum ($<10^{-6}$ Torr.) and furnace cooled. Both plates indicated a crystal structure of the disordered type when examined by x-ray diffraction. One of the plates was further treated by aging in a vacuum furnace (5×10^{-6} Torr.) at 710°C for 100 hours. According to Ellis and Greiner[35] such a treatment should provide an ordered body centered cubic structure (Type B2).

Diffraction patterns of the samples (plates, tensile and metallographic samples) removed from the aging furnace indicated relatively strong ordering diffraction peaks. Refering to Table 2 we see that the reflections of (hkl) indices (100), (111) and (210) are due to the ordering and are relatively weak due to the fact that the atomic scattering factor of iron and cobalt are within 3% of each other[37]. Diffraction from the surfaces of the ordered plate (Table 4) after polishing, e.g. wet papers to 650, dry paper to 3/0, wet alumina 1μ, Vilella's etch and polish with alumina 0.05μ for

for three cycles, indicated that the relatively strong ordering lines were significantly less than those observed on a metallographic sample (Table 3). A diffraction pattern from the edge of the plate, however, indicated that the preferred orientation in the plate was quite strong (Table 5) due to the casting techniques and that abnormal line intensities should be expected and be a function of orientation. A cursory analysis suggests that the (110) planes are normal to the surface of the plate. A detailed study of the fraction of orientation, however, has not been conducted, this being beyond the scope of the current program. There was a slight increase in hardness observed in the ordered structure - Rockwell B-82 (average of ten tests). The tension tests revealed that the alloy had become more brittle on ordering (Table 1). One tensile test specimen fractured while thread grinding the grips. The other two tests conducted showed very low values of fracture stress of 5,100 and 2,550 p.s.i. respectively, with the latter specimen fracturing in two regions.

Figures 2 and 3 are electron micrographs of the etched surfaces of an "as-cast" and ordered plate. The etching process does create a small degree of surface roughness which is evident from the micrographs. This roughness, however, is not as severe as the presence of holes and microporosity in the surface, which was probably due to the decrease in solubility of gases in one or both of the high purity metals when they were mixed during alloy preparation, or from gas pick-up from the adsorbed gases on the casting mold surfaces. The porosity is continuous throughout the bulk of the solid. Although the metals were prepared in vacuum, it

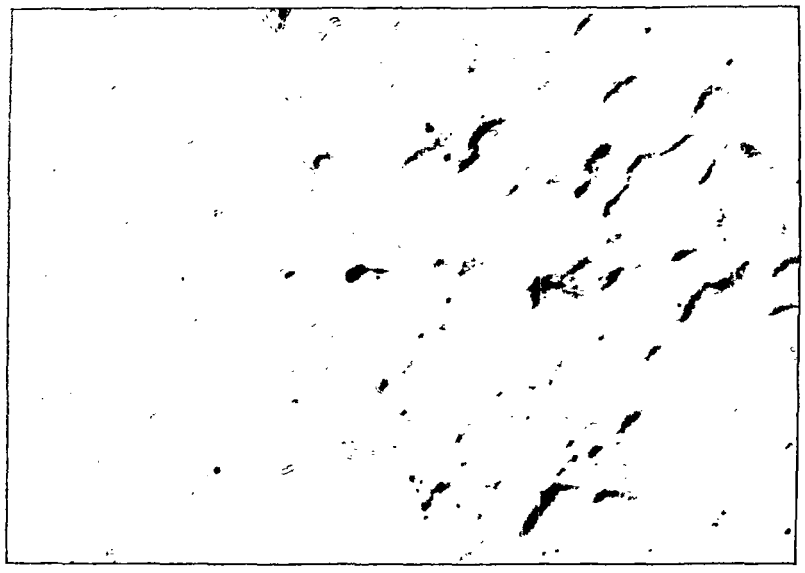

Magnification: 35,000

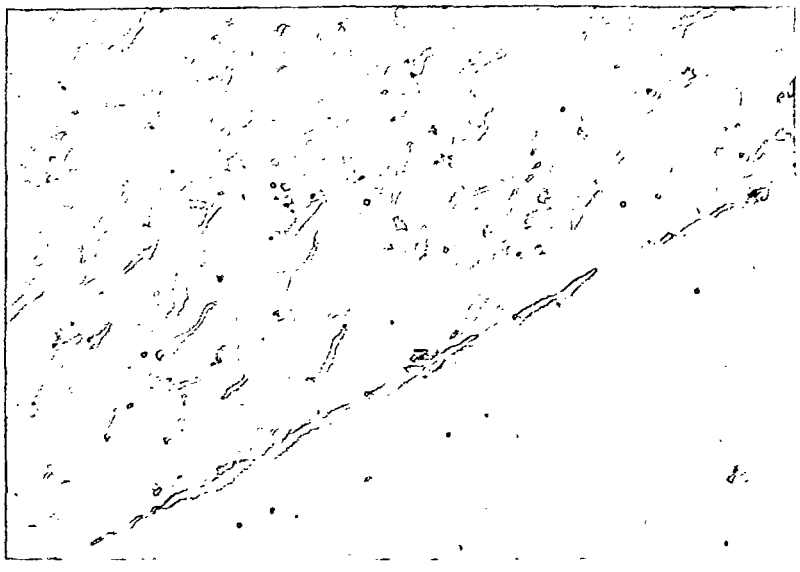

Magnification: 22,500

Figure 2: Electron Micrographs of grain boundaries in "as-cast" Co-50Fe alloy plate.

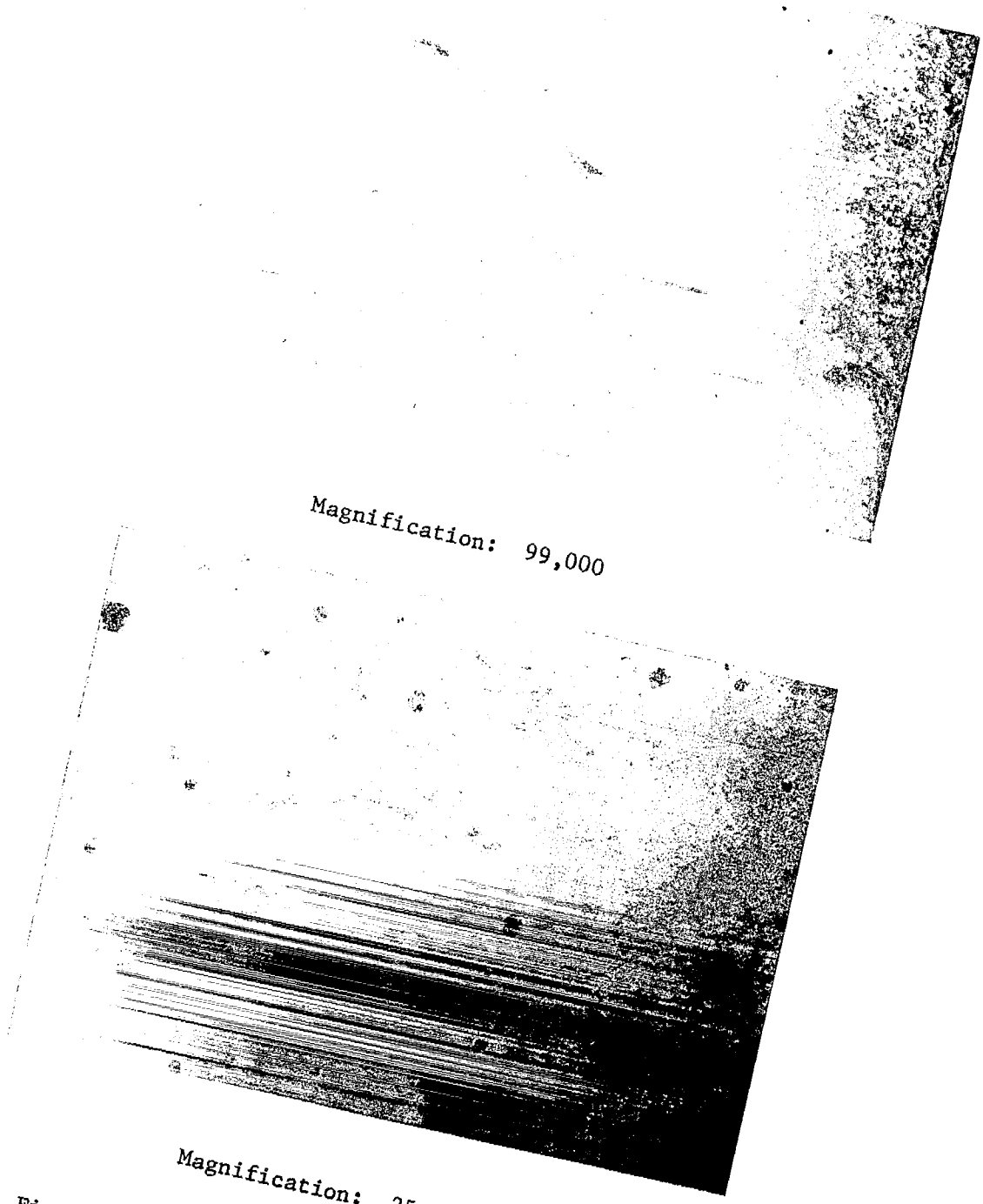

Magnification: 99,000

Magnification: 25,000

Figure 3: Electron Micrographs of grain boundary porosity in ordered Co-50Fe alloy.

could be that the cast ingots were not soaked in vacuum in the liquid state for an extended period which might have produced a lower degree of porosity in the bulk. The presence of porosity would result in a lower apparent value of the measured strength (17000 - 9000 p.s.i.), however, observations during the preparation of the adhesion samples (1/8 inch greater diameter) suggest that the inherent weakness in this material is due to a very low grain boundary strength. For example, even the most careful hand grinding techniques failed to produce two suitable rods for adhesion studies, even though nearly 150 attempts were made. In each case the rod eventually fractured under almost no stress along a grain boundary which traversed the rod diameter. One of the pairs of Co-50Fe alloy rods which was mounted in the adhesion cell for test collapsed under the very minimal stress imposed by the sample support rods, during the degassing operation. The mechanical properties which have just been considered, suggest that low coefficient of friction values are to be expected for this alloy.

Figure 4 demonstrates an interesting effect of the extreme brittleness of the Co-50Fe alloy. During the metallographic polishing a nearly perfect surface received one scratch from one silicon carbide crystal which extended the length of the plate. Microscopic examination of the single pass wear track clearly demonstrated the orientation effects of wear by the distribution of micro cracks etc. from grain to grain. Some grains were completely uneffected while adjacent grains to that which was uneffected appeared as in Figure 4.

Static adhesion tests on the Co-50Fe alloy were conducted after the

following treatment. Two cast bars (0.7 x 0.7 x 3 in.) of the alloy were work hardened by forging. The samples were heated to 1050°C i.e. well above the $\alpha \rightarrow \gamma$ transition temperature, and hammer forged until the temperature decreased to about 985°C, the onset of the brittle α-phase. The bars were reduced in several cycles by this method such that their overall length had about doubled. They were then cooled in the furnace, down to room temperature. The adhesion samples (rods of 1/16" diameter and 1" long) readily prepared from the finer grain material were mounted in the adhesion apparatus for further investigation.

A suitable specimen from the work hardened samples was subjected to x-ray diffraction using Chromium Kα radiation, the filter being vanadium. A glance at Table 6 shows that the presence of the reflections of (101), (200) and (211) correspond to the disordered body centered cubic structure, while the absence of (100), (111) and (210) indicate that no ordering had occured. Figures 5, 6, and 7 show optical micrographs of the Co-50Fe in the "as-cast", ordered and work-hardened conditions respectively. Figure 7a shows a micrograph of the alloy after completion of the adhesion tests.

The hardness of the work-hardened Co-Fe alloy was somewhat higher than the "as-cast" specimens. A hardness of Rockwell B-87 (average of ten tests) was observed, compared with Rockwell B-78 for "as-cast", which suggests that work hardening did not significantly change the mechanical properties of the alloy although the grain boundaries were strengthened sufficiently for making adhesion samples.

Magnification: 4,200

Figure 4: Electron Micrograph of grain boundary and a scratch (made with SiC crystal and 1μ wide) in polished "as-cast" Co-50Fe alloy plate.

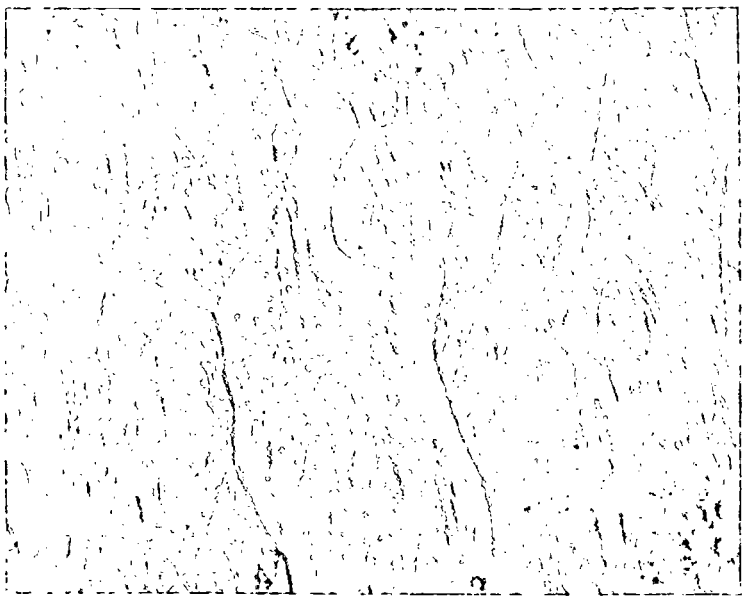

Magnification: 75

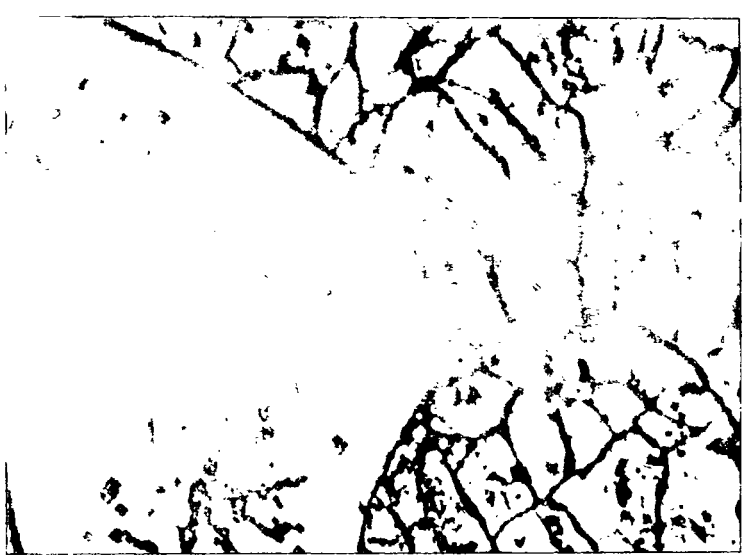

Magnification: 250

Figure 5: Optical Micrographs of "as-cast" Co-50Fe alloy.
Etchent: Vilella Reagent.

Note the sub-boundaries made up of etch pits.

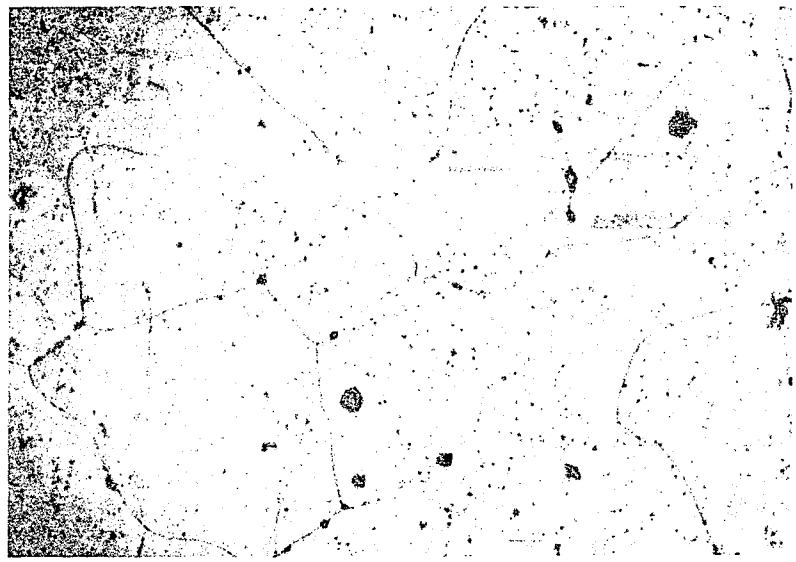

Magnification: 75

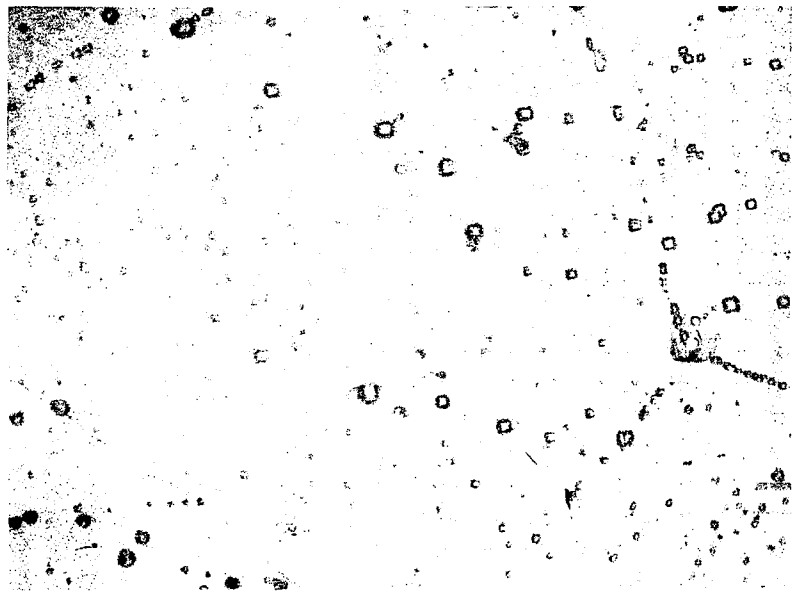

Magnification: 250

Figure 6: Optical Micrographs of ordered Co-50Fe alloy
Etchent: Electrolytic (5% H_3PO_4, 95% H_2O).
Note the presence of sub-boundaries, but to a lesser degree than the "as-cast" specimen.

Magnification: 100

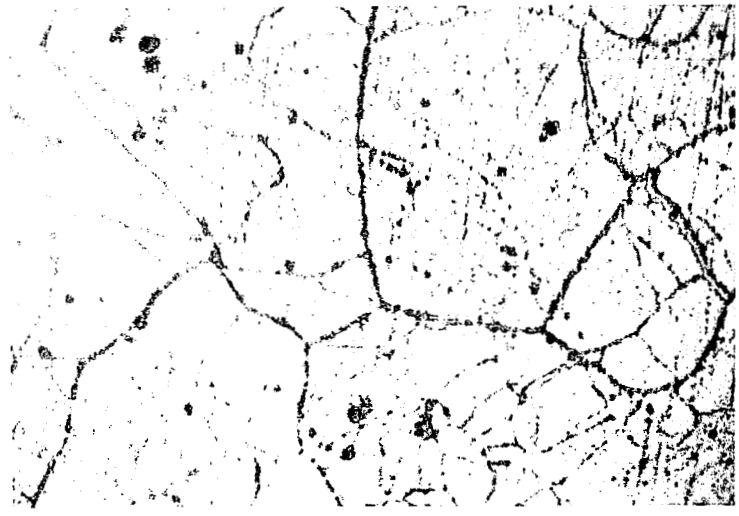

Magnification: 500

Figure 7: Optical Micrographs of work hardened Co-50Fe alloy.
Etchent: Vilella Reagent

Note the smaller grain size as compared with the "as-cast" alloy.

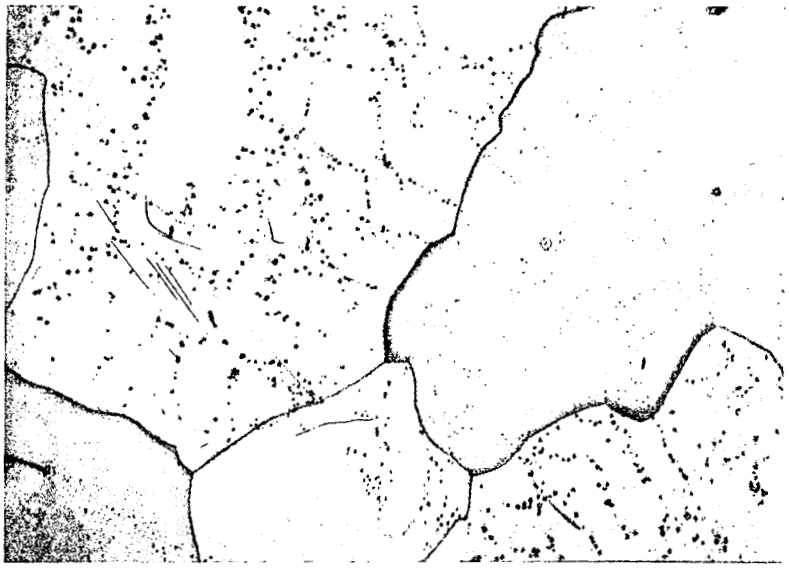

Magnification: 100

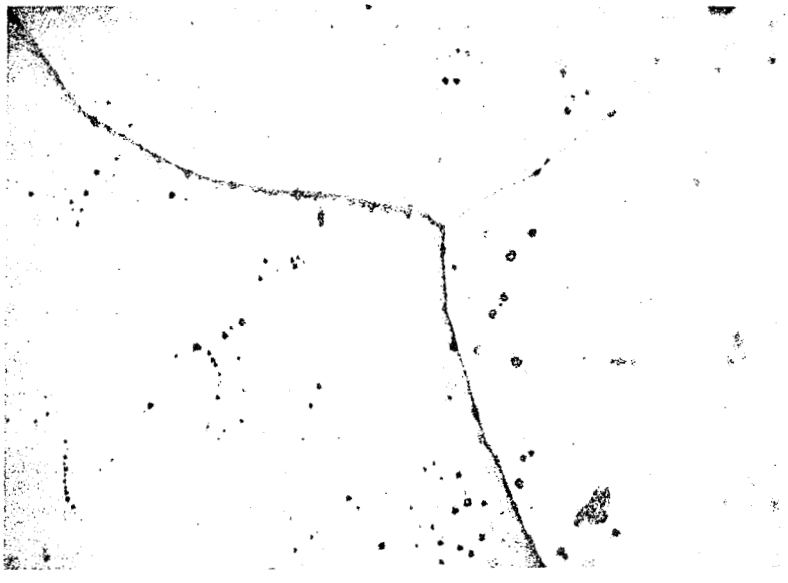

Magnification: 500

Figure 7a: Optical Micrographs of the adhesion specimens of Co-50Fe, (made from work hardened material) after the adhesion test. Etchent: Electrolytic (5% H_3PO_4, 95% H_2O). Note that grains are larger than in Figure 7, due to thermal degassing.

Cobalt - 25 Molybdenum - 10 Chromium System

As already mentioned, the Co-25Mo-10Cr alloy in the "as-cast" condition had a hardness value of Rockwell C-49 and was quite susceptible to micro-cracking due to thermal stresses; such, was based on observations during the cast plate size reduction. The mechanical properties of samples commercially solution treated in vacuum for 60 hours at 1200°C (and air cooled) which appeared to be without prior defects or thermal cracks by fracture, on surface inspection, are as follows:

Young's Modulus	:	$29\text{-}32 \times 10^6$ p.s.i.
Yield Point	:	1.37×10^4 p.s.i.
Fracture Stress	:	2.80×10^4 p.s.i.
Hardness	:	C-47 (Rockwell)
Reduction in Area	:	Nil

The fracture surface structure was typical of brittle fracture. Various specimens of the Co-25Mo-10Cr alloy were subjected to annealing in vacuum (10^{-6} Torr) at 1220°C for 116 hours, and aging at 700°C and 800°C for 50 and 61 hours respectively. For all these treatments, the specimens were subjected to X-ray diffraction (Table 7), tension and hardness tests (Table 8) and metallography (Figures 9 to 11). Figure 12 is an optical micrograph of the Co-25Mo-10Cr alloy which has been commercially heat treated in vacuum at 1200°C for 60 hours and air cooled. It shows a two phase structure and there is hardly any evidence of a third phase. This is due to the relatively rapid cooling rate attained by air cooling, which prevented the precipitation of a third phase. Comparing this with Figure 9 which shows the microstructure of the alloy subjected to nearly the same treatment, except that it is furnace

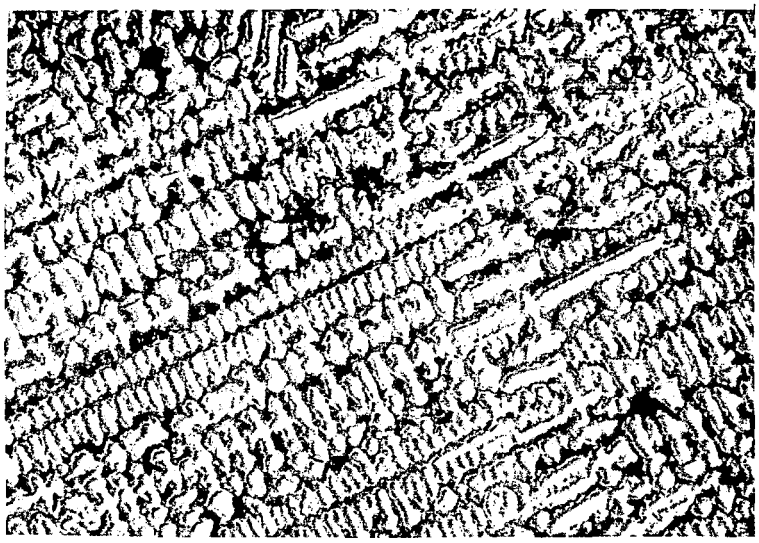

Magnification: 100

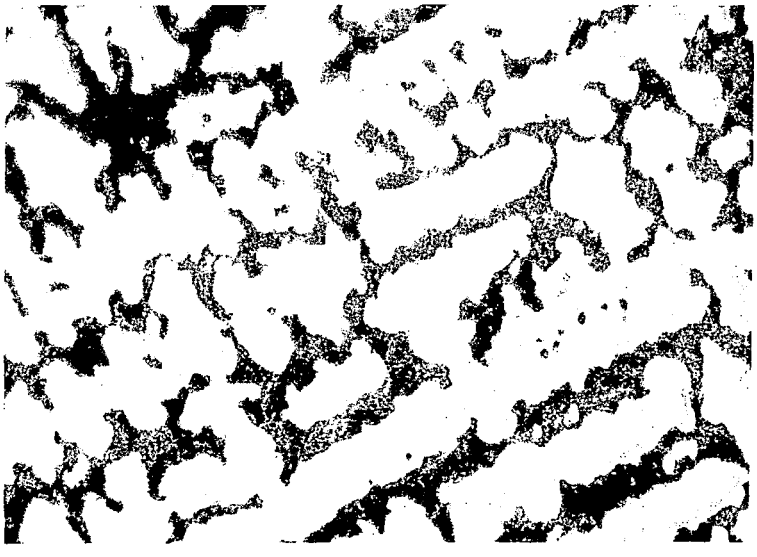

Magnification: 300

Figure 8: Optical Micrographs of "as-cast" Co-25Mo-10Cr alloy
Etchent: Electrolytic (5% H_3PO_4, 95% H_2O).

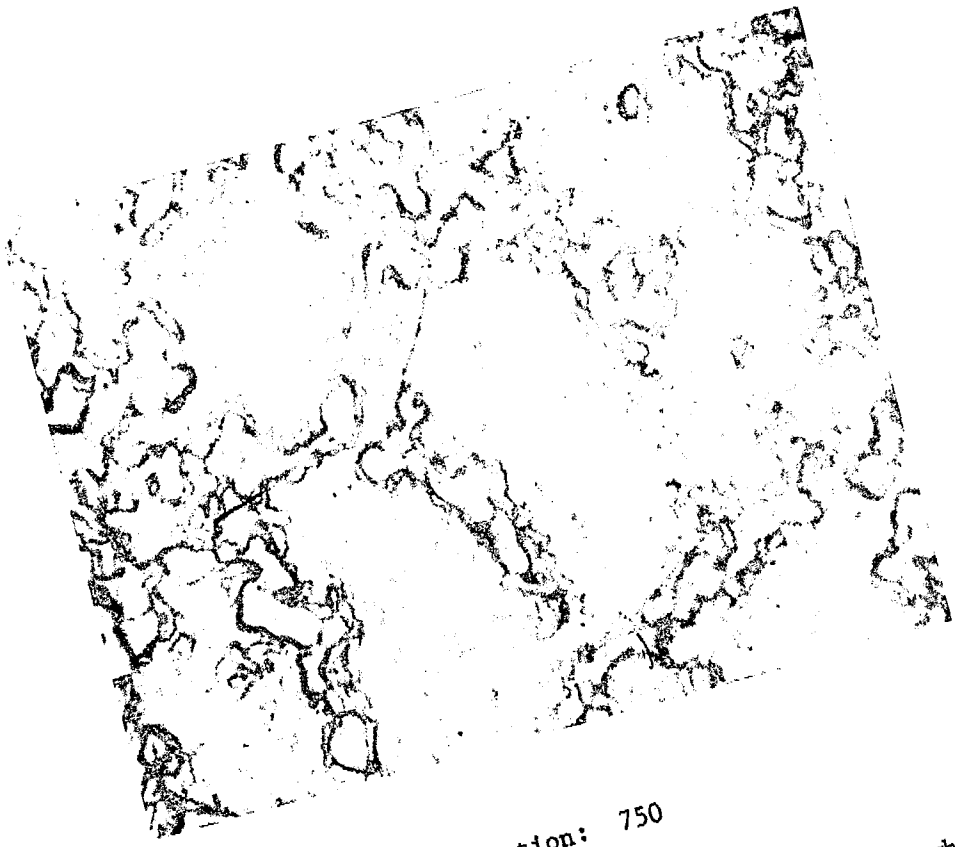

Magnification: 750

Figure 9: Optical Micrograph of Co-25Mo-10Cr alloy which has been annealed in vacuum (10^{-6} Torr) at 1220°C for 116 hours. Etchent: Same as in Figure 8. Note the precipitation of the third phase due to slow cooling in the vacuum furnace.

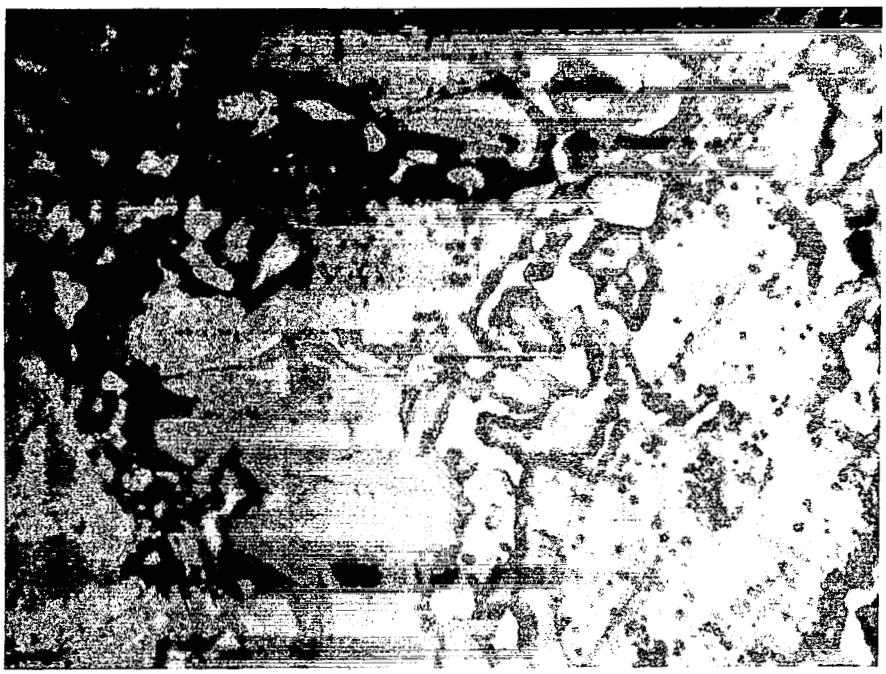

Magnification: 750

Figure 10: Optical Micrograph of Co-25Mo-10Cr alloy which has been aged at 700°C for 50 hours in vacuum (10^{-6} Torr), after commerical heat treatment at 1200°C for 60 hours and air cooled.
Etchent: Same as in Figure 8.
Note the third phase precipitates.

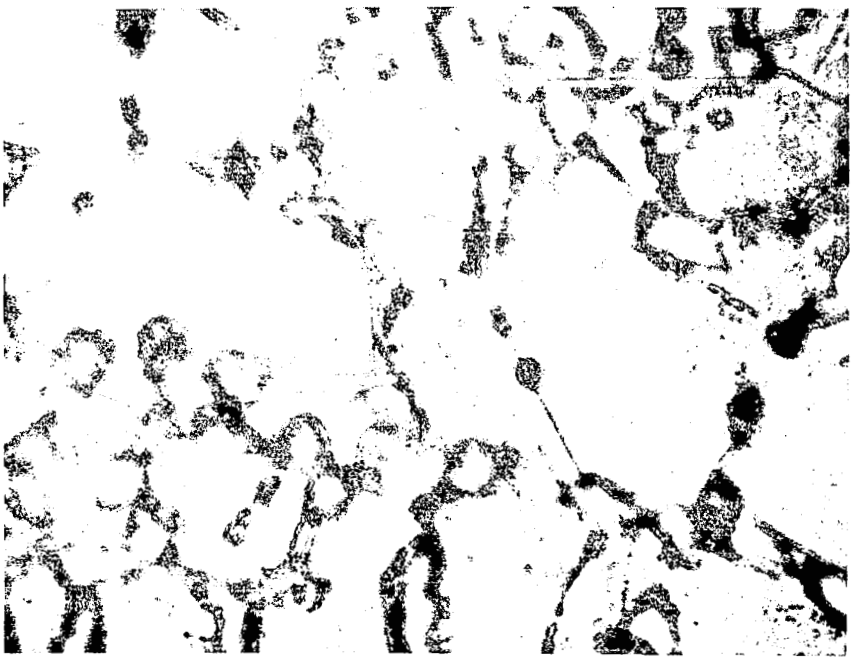

Magnification: 750

Figure 11: Optical micrograph of Co-25Mo-10Cr alloy which has been aged at 800°C for 61 hours in vacuum (10^{-6} Torr), after commercial heat treatment at 1200° for 60 hours and air cooled.
Etchent: Same as in Figure 8.
Note more precipitation of the third phase.

Magnification: 750

Figure 12: Optical Micrograph of Co-25Mo-10Cr alloy which has been commercially heat treated in vacuum at 1200°C for 60 hours and air cooled.
Etchent: Same as in Figure 8.
Note the two phase structure, the cooling rate in air being sufficient to prevent the precipitation of the third phase.

cooled, there is a considerable amount of a third phase precipitated. Figures 10 and 11 are the microstructures of the alloy, aged at 700°C and 800°C respectively and shows the precipitation of the third phase in different stages, the latter treatment having more of precipitation. Figure 8 shows the dentritic structure of the "as-cast" alloy with clear evidence of a third phase.

The ternary phase diagram of Co-Mo-Cr has not been completed for the compositional range of the alloys of interest in this investigation. However, through the use of a rather complete 1200°C isothermal section[38] and the completed Co-Mo binary phase diagram[35], sufficient extrapolation can be accepted for a reasonable interpretation of the structure data obtained from the alloy under investigation. The 1200°C isothermal section (Co-Mo-Cr) indicates that the (α Cobalt + μ phase) field exists within the composition limits Co + 18 to 55 Mo + 0 to 12 Cr. The μ phase from the binary system data is given by the composition Co_7Mo_6 and according to Lux et al.[39], the addition of chromium generates substitution in the μ phase in the form of $Co_7Mo_xCr_y$ where x varies from 4.7 (1000°C heat treatment) to 5.2 (800°C heat treatment) and y varies from 1.74 to 2.5 respectively. From the binary phase diagram of Co-Mo (Figure 13) at 25 w/o Mo, the anticipated phases upon cooling from the solidus are α-Co (stability range of about 100°C), α-Co plus μ-phase (stability range about 300°C) and ε-Co plus Co_3Mo (to room temperature from about 980°C). There is some doubt about an unstable and unknown compound which exists only in the range of 1200°C. Alloys in the immediate composition range of Co-25Mo-10Cr would

be most difficult to place in the α-Co solid solution condition (T≈1300°C) since the very narrow range of α is adjacent to the liquidus temperature (1350°C); and as a consequence, annealing at 1220°C for 116 hours accomplished little more than μ-phase particle refinement and compositional equilibration. The hardening effects, if any, should only be accounted for through μ phase decomposition in the peritectic reaction to Co_3Mo. which would be expected to be very sluggish, and also by the α-Co → ε-Co (hexagonal) transformation. The observations of this investigation bear out these expectations. For example, none of the heat treated conditions have indicated a significant quantity of Co_3Mo which is uniquely characterized by a strong diffraction line at about 3.00 A° and a medium intensity line at 2.54A° [40] as indicated in Table 7. The μ-phase, on the other hand, is clearly characterized in all the samples. The inability to place the alloy in the α solid solution range (without jeopardy to the vacuum furnace due to melting), immediately limits the ability to utilize solid state precipitation as a hardening reaction. For example, annealing at 1220°C for 116 hours did not vary the hardness (R_c = 50±3) of the Co-25Mo-10Cr alloys significantly and so was the case after aging at 700° and 800°C for 50 and 61 hours respectively (Table 8). This was unlike what was observed by Lux et al.[39] who found for Co-20Mo-12Cr alloy, a hardness value of R_c=26 after solution treatment at 1200°C for 100 hours and thereafter air cooling, which proved to dissolve most of precipitates present in the "as-cast" structure. The decrease in composition of 5 w/o Mo shifts the 1200°C solution treated structure into α-Co solid solution range such that proportional amounts

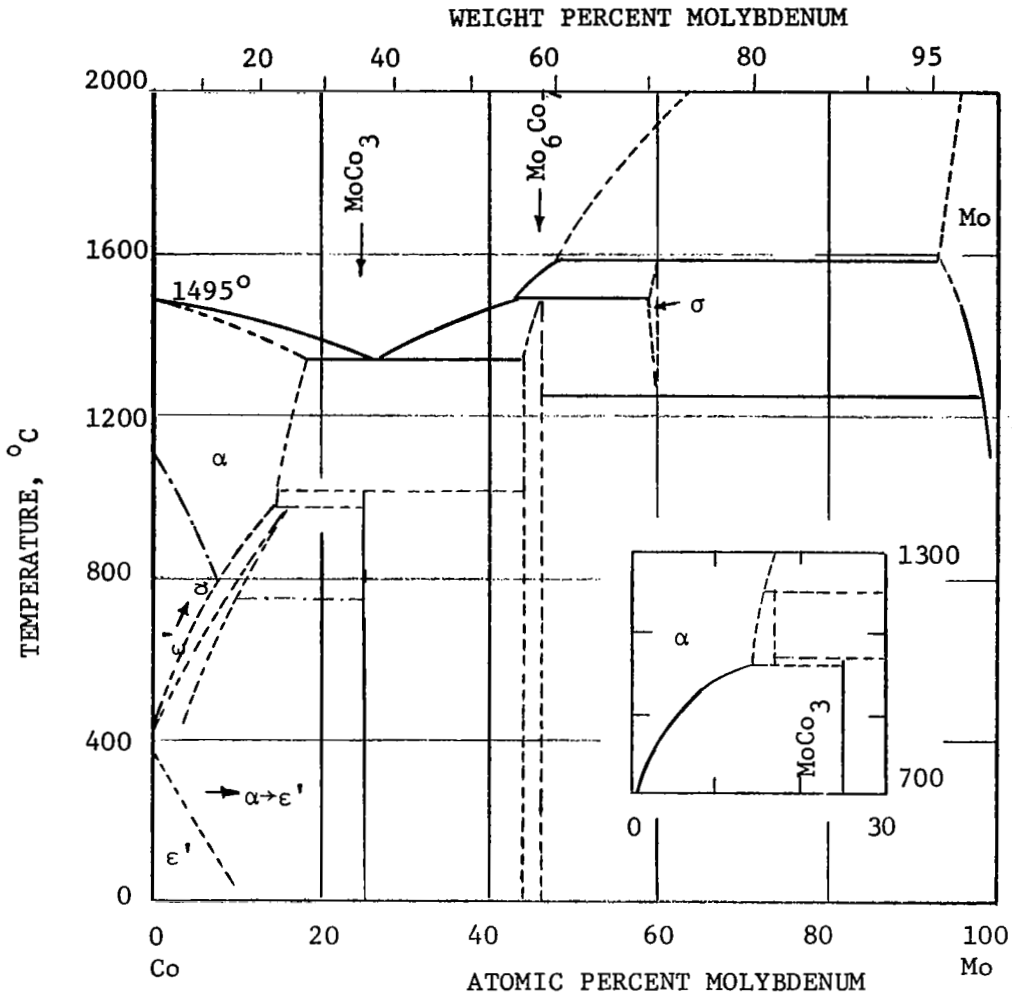

Figure 13: The cobalt-molybdenum equilibrium diagram, (Hansen[36]).

of μ phase and $CoMo_3$ can be developed through an ordinary precipitation process. This is evident from their hardness data:

Alloy	Condition	Hardness Rockwell C
Co-20Mo-12Cr	As Cast	46
	Solution Treated ($1200^{\circ}C$ for 100 hrs. and air cooled)	26
	Aged $600^{\circ}C$, 100 hours	28
	Aged $800^{\circ}C$, 100 hours	50
	Aged $1000^{\circ}C$, 100 hours	50

The heat treating time curves also presented by Lux et al.[39] indicate that full hardness can be developed within 10 hours.

In conclusion, it was felt that sufficient hardness could be achieved if the Mo concentration was decreased to 22 w/o or less such that a significant α-Co field is available below the liquidus to permit safe solution treatment (1250 - $1275^{\circ}C$) and in turn allow precipitation reactions. Quite possibly, the numerous internal cracks observed in the Co-25Mo-10Cr alloys were due to the extreme hardness developed by the eutectic precipitate phase at or very near the liquidus ($1340^{\circ}C$). If a large solution field of relatively soft or ductile α-Co were present over a wide temperature range, the excessive thermal stresses on cooling could be relieved prior to the initiation of the hardening reactions. This would be illustrated by reducing the Mo content to at least 22 w/o, and a comparison of the crack population in each case ought to confirm the prediction. If no internal cracks are available, one ought also to expect a significant increase in fracture strength due to the loss of the internal stress concentrations, i.e. cracks.

Static adhesion tests were conducted on this alloy in ultra high vacuum and presented by Chung.

Apparatus:

The adhesion experiments were conducted in an ultra high vacuum apparatus which was almost identical to that described in detail by McNicholas[41]. The only significant change was the redesign of the adhesion cell to include nearly all metal components. This modification was used only for the study of Co-50Fe alloy while the Co-25Mo-10Cr alloy was investigated with the older design of the adhesion cell as described by McNicholas. The redesigned adhesion cell is illustrated schematically in Figure 14. The adhesion cell was constructed from a 1-1/2" Varian double cross, a Varian cross and a Varian Tee, all connected in series as illustrated. Attached to the 1-1/2" Varian double cross was the diffusion pump vacuum system (P) which was connected through a 1-1/2" Tee varian control value (N). Other attachments to the Varian double cross include a titanium sublimation pump (E) and a Granville - Phillips Ion Gauge (F) mounted in line of sight with the sample. One end of the Varian control valve (N) was connected to a Granville-Phillips 1" UHV value (M) which isolated the spectrographically pure argon source (L).

One of the 2mm x 25mm Co-50Fe samples (A) was fixed as shown in Fig. 14, while the second was mounted on a ceramic support rod (B) which formed one end of a torsion balance beam with electrical leads mounted as shown. The torsion beam was supported on a 0.3 mm tungsten wire fixed between two 5 mm stainless steel rods forming a bracket which in turn was welded to the Conflat flange base of the cell. The flange also supported two electrical feed throughs

for the sample leads (C). A magnetic rod (J) was mounted on the torsion beam at the end opposite the sample such that the position of the torsion beam, i.e. the sample at the end of the torsion beam, could be positioned relative to the fixed sample by use of an external magnet (H). For example, during argon ion bombardment (AIB) cleaning, as much as 25 mm sample separation could be achieved, while to initiate an adhesion cycle, 1 mm separation could be fixed between the two. The torsion beam was moved from the fixed 1 mm sample separation distance into a known contact load by increasing the current in the external solenoid (K) which interacted with the magnet (J) which was supported on the end of the torsion beam by means of a straight wire strain guage. The 0.023 mm tungsten strain guage was welded at each end to 2 mm silver wire leads which were then welded to the leads of the through seal (G).

The load between the samples was applied at a linear rate of about 1.5 grams/min. by varying the 110 VAC input to a DC power supply which provided current to the solenoid (K). The DC power supply with 110 VAC input was preset to provide the necessary current for the desired maximum contact load between the samples. The variac was then motor driven between 110-0-110 VAC such that the DC output to the solenoid varied between the preset maximum load and zero.

The load necessary to shear the stationary magnetic force fixing the samples at the position of 1 mm separation was available to provide a tensile fracture force when the unloading cycle was complete. The zero load contact point was determined as that point at which the contact resistance varied from infinity as detected by the first motion of a high resistance meter on

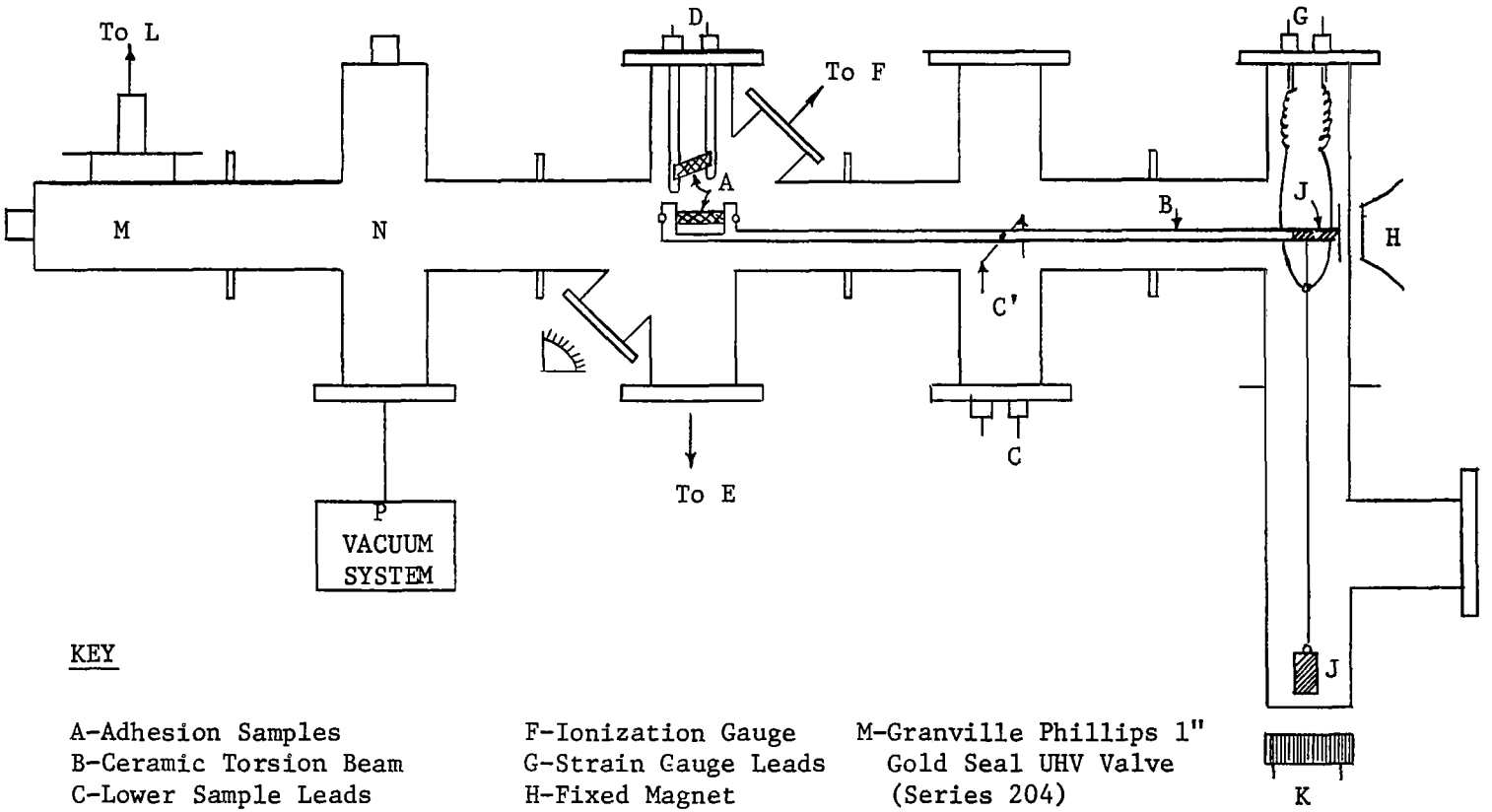

KEY

A-Adhesion Samples
B-Ceramic Torsion Beam
C-Lower Sample Leads
C'-Torsion Beam Pivot
D-Fixed Sample Leads
E-Titanium Sublimation Pump
F-Ionization Gauge
G-Strain Gauge Leads
H-Fixed Magnet
J-Iron Slugs
K-Solenoid
L-Source of Argon
M-Granville Phillips 1" Gold Seal UHV Valve (Series 204)
N-1/2" TEE Valve (Bakable)
P-Vacuum System

Figure 14: Adhesion Cell.

the 100 KΩ scale. A Sanborn transducer-amplifier (No. 312) was used in conjunction with the strain guage to monitor the impressed loads which rarely exceed four grams. The output of the transducer provided an input to the x-axis of the x-y recorder. The strain guage system was calibrated in grams by removing the fixed upper sample and replacing it with a differential transformer transducer which had been calibrated in grams. The sensitivity of the force measuring system was within ±0.01 gram.

The contact resistance measuring circuit is shown in Figure 15. The contact resistance between the samples was detected continuously utilizing a L & N Precision Kelvin Bridge with a Keithley nanovoltmeter (No. 148) as a null indicator. Voltage impressed across the contact resistance was six millivolts (open circuit) which was well within the limits, discussed by McNicholas[41], to prevent contact burning. The output of the null indicator was used as the input to the "y" function of an x-y recorder and indicated the values of contact resistance. This was accomplished by adjusting the bridge resistance such that at maximum load, i.e. minimum resistance, the null indicator indicated a balance point or no current flow. Any deviation from the null point in a positive direction indicated a higher contact resistance which was calibrated over the entire range by substitution of secondary standards directly in place of the crossed wire samples. NBS primary standards of 0.01 and 0.10 ohms were situated in the circuit to enable a periodic check of the apparatus to the x-y record.

Procedures

The Co-50Fe samples, subjected to the treatment mentioned earlier, were mounted in the adhesion cell, the system evacuated to below 10^{-6} Torr and the 400°C, ten hour bake-out cycle initiated. After bakeout and a thorough outgassing of the ionisation guage filaments, sorption pump and samples e.g. ambient pressure below 10^{-8} Torr. at 900°C, the system pressure remained static at about 3×10^{-9} Torr. About 50 adhesion cycles, e.g. zero load - peak load - fracture, utilizing these unclean (without argon ion bombardment) Co-50Fe samples, were generated.

Spectrographically pure argon was then admitted to the system to a pressure in the range of 5×10^{-4} Torr, and argon ion bombardment (AIB) cleaning of the sample surfaces was initiated by placing a DC potential of about 500 volts between the samples (-) and the plate. A current of about 0.2 ma/mm^2 was maintained on each sample for at least one half hour to remove surface oxides. The residual argon gas was then evacuated and the samples were again annealed above 900°C for at least half an hour each to remove adsorbed gases and surface defects. AIB cleaning and annealing cycles were then alternatively used until samples were clean, e.g. c.f. Keller - McNicholas[13]. About 150 adhesion cycles e.g. zero load - peak load - fracture, utilizing clean Co-50Fe samples were recorded for different loads. Adhesion runs of clean surfaces were recorded after argon ion bombardment in argon and after evacuation of the argon to ultra high vacuum (UHV) and sample anneal to at least 900°C.

For the analysis of the adhesion data for the unclean Co-50Fe samples,

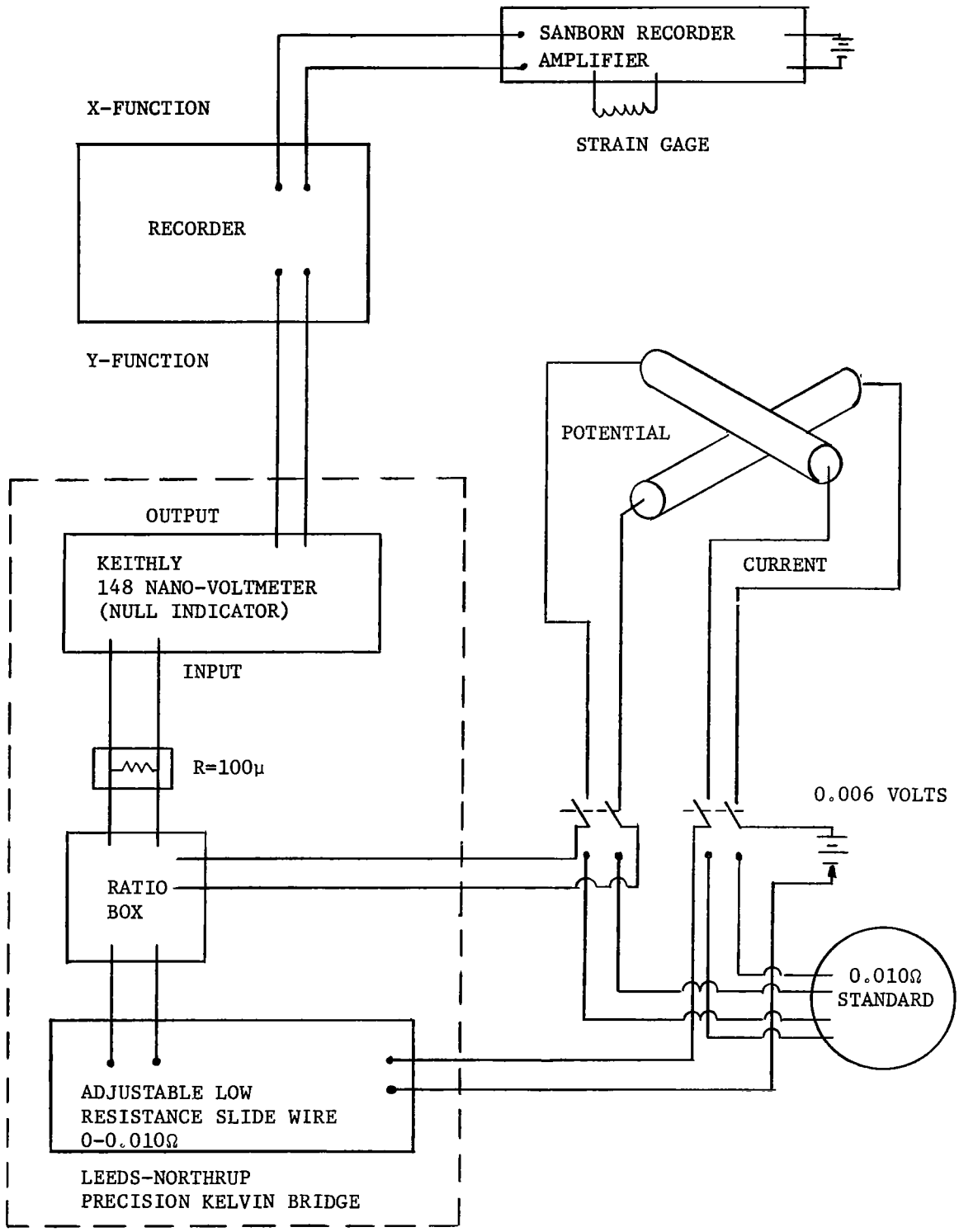

Figure 15: Recording Circuit

(i.e. without Argon ion bombardment and only thermal degassing) the assumption was made that one strain guage unit is approximately equal to one gram, within a 10% error, since precise calibration of the strain guage units into grams had to be made only after experiments were completed and the cell disassembled. The adhesion data for the cleaned samples (after AIB) were analyzed after precise calibration of the strain guage units into grams. It was found that one strain guage unit is equivalent to 0.92 grams.

The resistivity value of the Co-50Fe to be inserted into equation 15 was taken to be the weighted average of the bulk resistivities of Co and Fe[31], which is 8 $\mu\Omega$-cm.

Tables 9 and 10 give the data from two of the many adhesion runs utilizing Co-50Fe couples which were thermally degassed but not argon ion cleaned. The observed resistance - load curves are shown in Figures 16 and 17 and traced from the original recording. Figures 19 and 20 show the static apparent stress versus strain curves plotted for the adhesion runs shown in Figures 16 and 17 respectively. Figures 22 to 28 represent static adhesion apparent stress-strain curves for seven of the most representative adhesion runs under various cleaning conditions (i.e. argon ion bombardment and annealing).

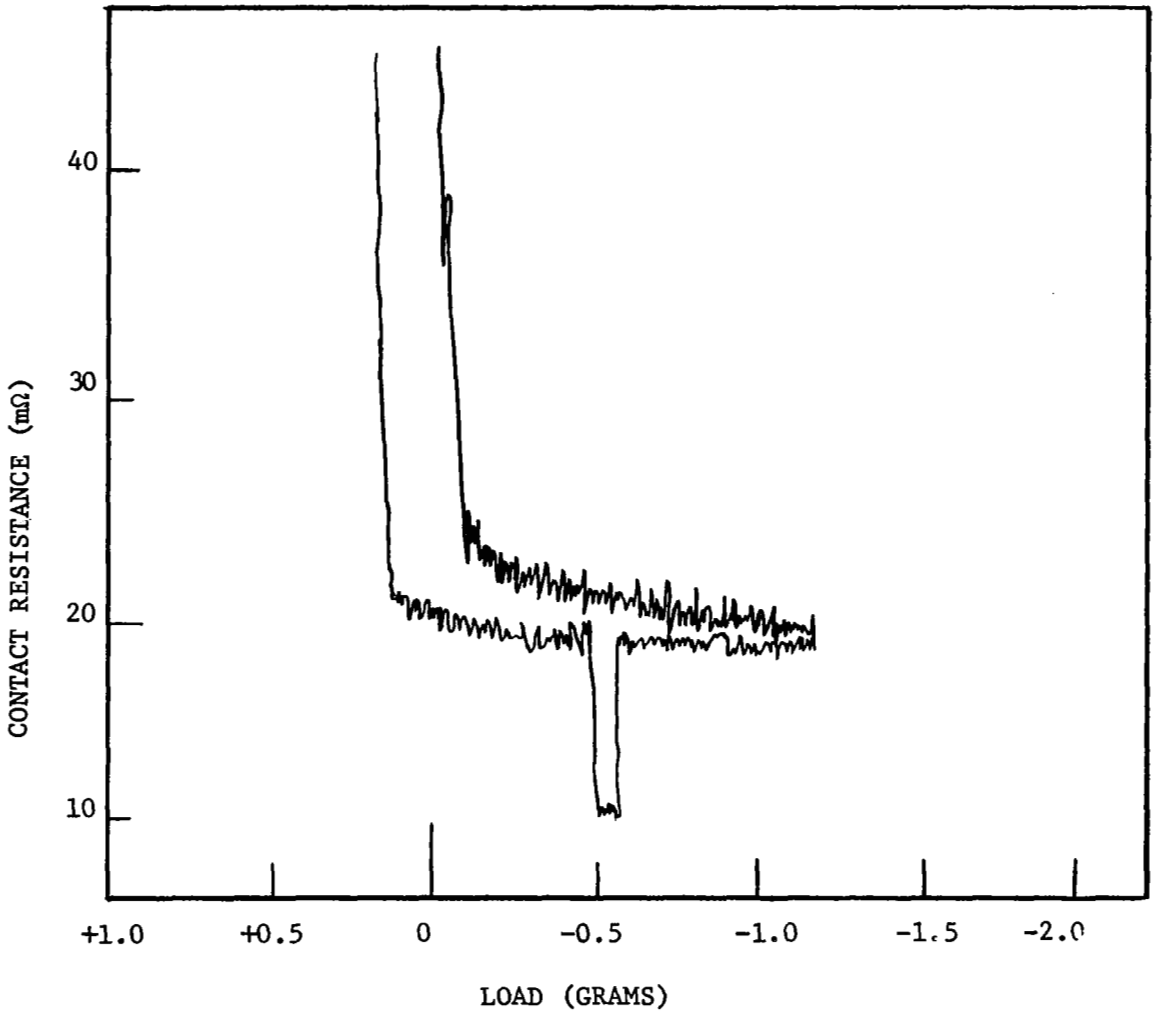

Figure 16: Contact Resistance Versus Static Load For Co-50Fe

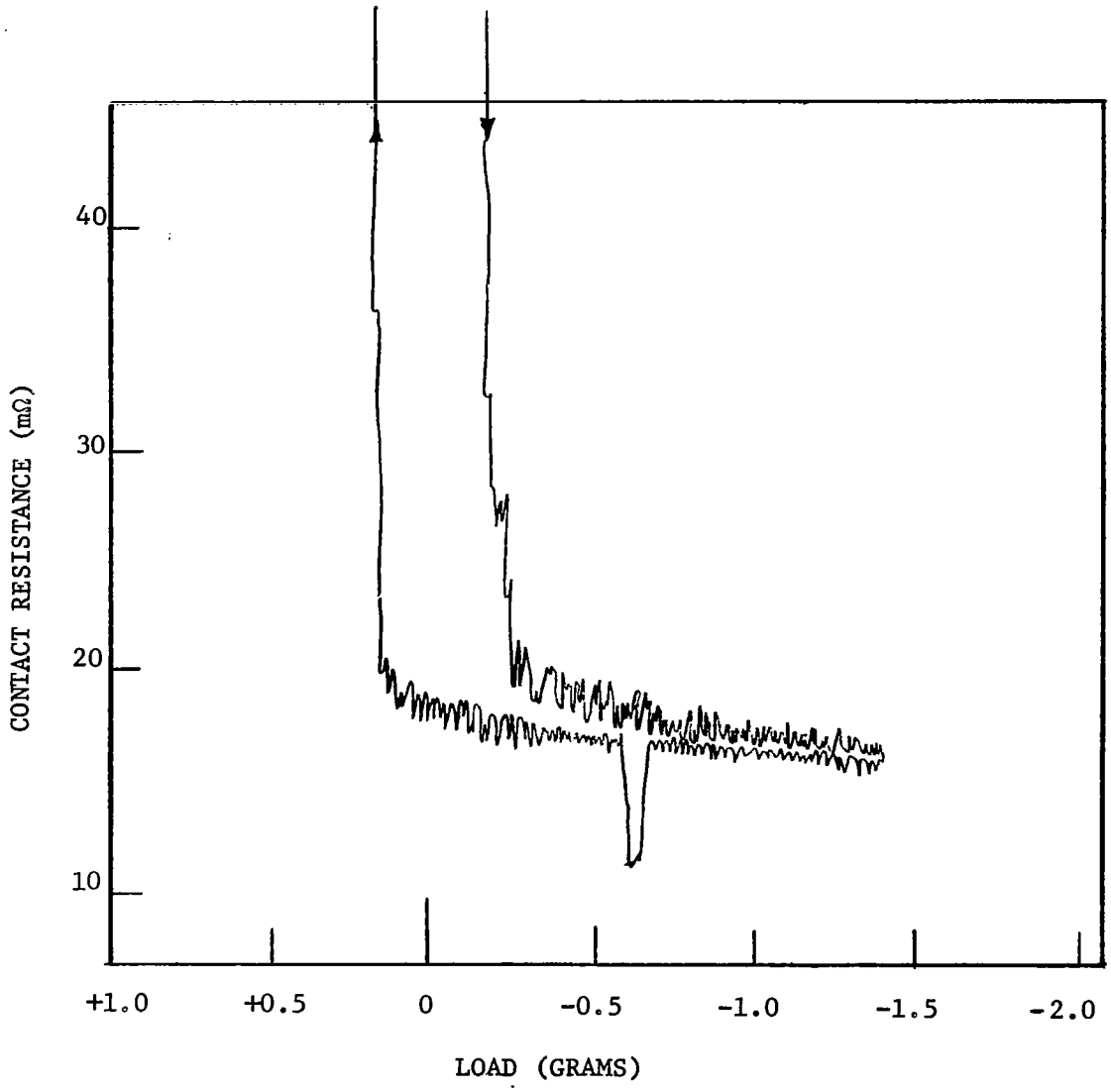

Figure 17: Contact Resistance Versus Static Load For Co-50Fe

RESULTS AND DISCUSSION

Cobalt - 50% Iron

Our discussion will begin with the interpretation of the static adhesion apparent stress-strain curves as determined from the contact resistance vs. load recordings. A typical plot in Figure 18 illustrates that after initiation of physical contact at zero stress and as the load is increased, the curve shape to the peak compressive stress identifies how the multitude of asperities are available to support the load to a bulk elastic manner, i.e. the interfacial plasticity has decreased and area expansion is due to an elastic response of the bulk. Considering Figure 18, throughout the investigation of several metal systems, contact fracture from the peak stress generally falls into one of the three categories sketched as cases A, B and C in Figure 18. Each case is a response of the real contact area to the released elastic stresses in the interface system. In case A, for example, the real contact area changes only by the variation due to elastic recovery of that area, that is the slope of the curve from peak stress to the tensile yield point is the Elastic Modulus of the material. The tensile part of this curve is the standard stress-strain diagram of the work hardened metal, with a yield point and fracture stress.

In the event the metallic contact area is specifically oriented, fracture sensitive to the severe notches in the contact zone or contaminated with a brittle phase, the build up of elastic stress as the load is released may become sufficient to permit a crack to propagate and thus reduce the real contact area. This would be evidenced by a decrease in strain which exceeds that decrease rate predicted by the Elastic Modulus. Case B illustrates a

situation in which the interface withstands a fraction of pressure release prior to fracture initiation and the remaining material providing some tensile strength. Case C, however, illustrates an extreme situation in which nearly all of the elastic contact is recovered as the pressure is released. This case is representative of a good bearing material from the standpoint of adhesion; Case A is the diametric opposite, since tangential motion can only serve to increase the contact area, i.e. increase the strain and improve the welded junction.

Figures 19 and 20 illustrate the apparent compressive stress vs. strain curves as determined from the contact resistance vs. load recordings of Co-50Fe crossed rods. The strain variation represents the true area change during contact due to the collapse of asperities as the stress increases. During loading, those asperities constituting the area of contact are deformed plastically and a rapid expansion in area is observed until a point is reached whereupon the bulk material supports a major fraction of the impressed load elastically. Each of the contact junctions, the number of which rapidly approaches an average value of 30 for this system during loading below the bulk elastic limit, is considered as a region of continuous metal. During unloading, these contacts experience elastic relief followed by normal tensile fracture behavior. The compression of crossed wires of Co-50Fe subjected only to thermal degassing (and not as yet Argon ion bombardment) very closely resembled a state of near atomic cleanliness as is evident from Figures 19 and 20. The observed data supports the asperity interaction model in that the apparent stress-strain data (Figures 19 and 20) demonstrates a stage of immediate

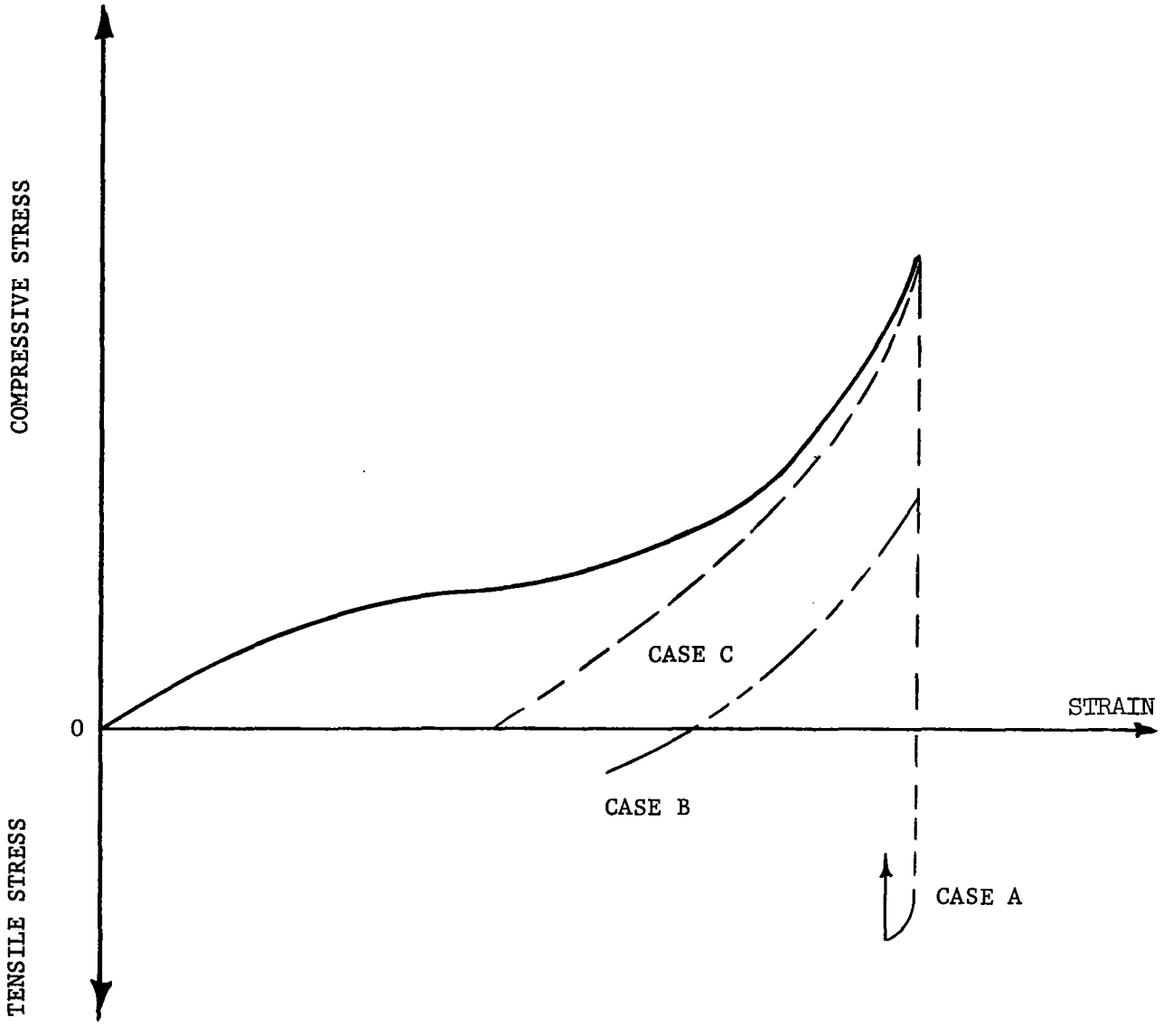

Figure 18: Static Adhesion Apparent Stress-Strain Diagram.

plastic deformation (high strain) upon loading which is continued over most of the range of applied load. The data suggests that severe deformation of these asperity junctions occurs before the load is substantially borne elastically by the bulk material as represented by the very steep portions of the curve at high strain values (i.e. 90% strain and 130% strain in Figures 19 and 20 respectively). The slopes in this portion are nearly that of Elastic Modulus for Co-50Fe, i.e. 28 x 10^6 p.s.i. Another interesting feature was that the welded junction separated by what appears to be a ductile fracture as is evidenced by the tensile portions of curves 19 and 20. Also, in Figures 16 and 17 it is seen that the contact resistance increases slowly i.e. contact area decreases as the tensile region is reached, which is characteristic of a ductile fracture. Two plausible explanations are evident depending on the exact state of the surface contamination at the instant of fracture. If no contaminants were present in the interface system, one might argue that the severe metal working developed by preforming multicontacts and fractures would develop a rather high concentration of defects in the contact region (10 μ^2) such that ductile fracture could be promoted. The initial contact of the same area of an extensively annealed single crystal surface on the other hand, might not provide a sufficient number of defects to permit ductile fracture, and as a consequence could fracture in a brittle manner, though no such fracture was observed in any of the fifty static adhesion runs taken after extensive degassing (annealing) of the samples. This could most probably be due to the very large number of dislocations generated while Co-50Fe bars were work hardened prior to sample preparation

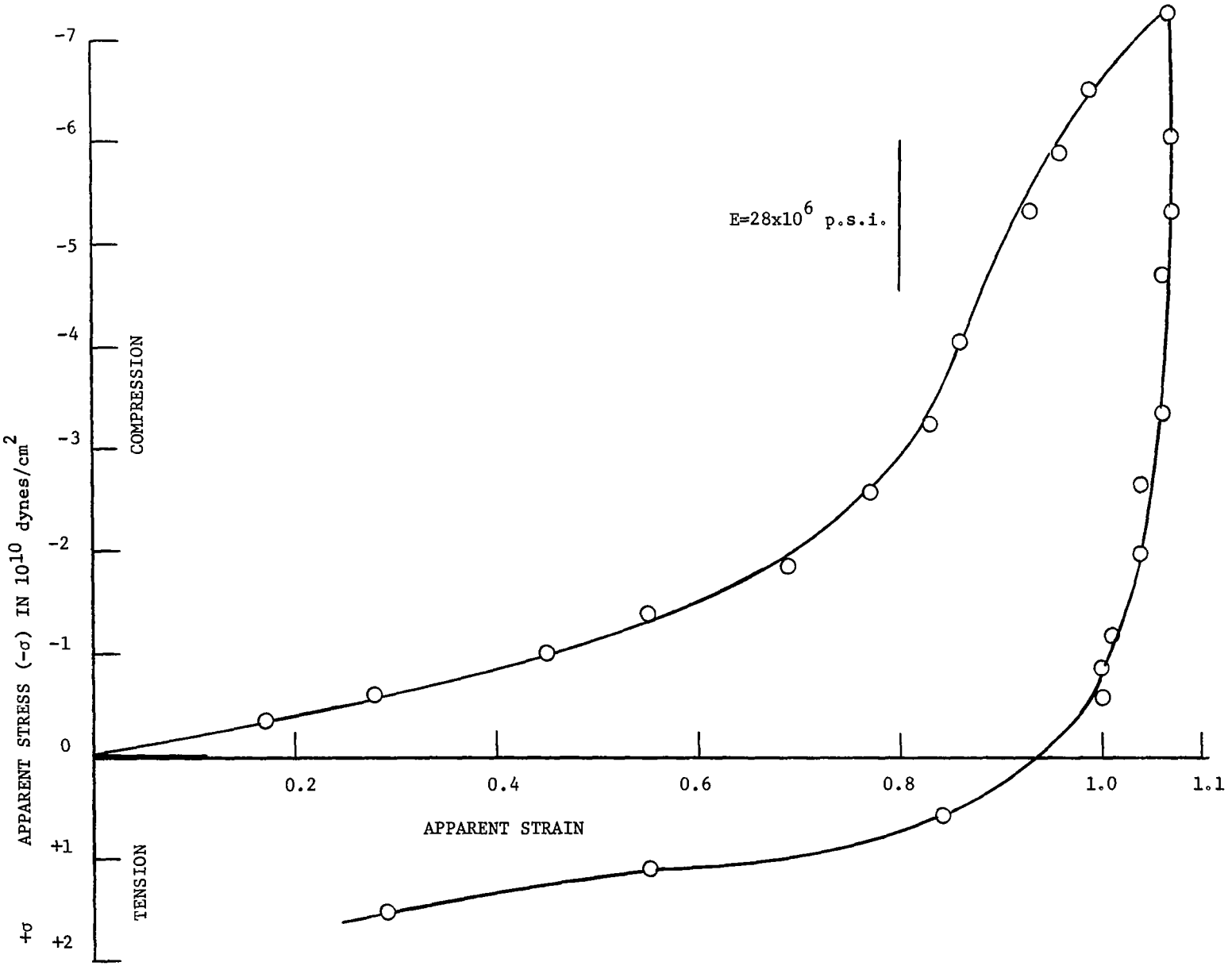

Figure 19: Static Adhesion Apparent Stress vs. Strain Diagram for Unclean Co-50Fe, in U.H.V. and at Room Temperature.
Maximum load: 1.3 grams, Minimum resistance: 18.9mΩ.

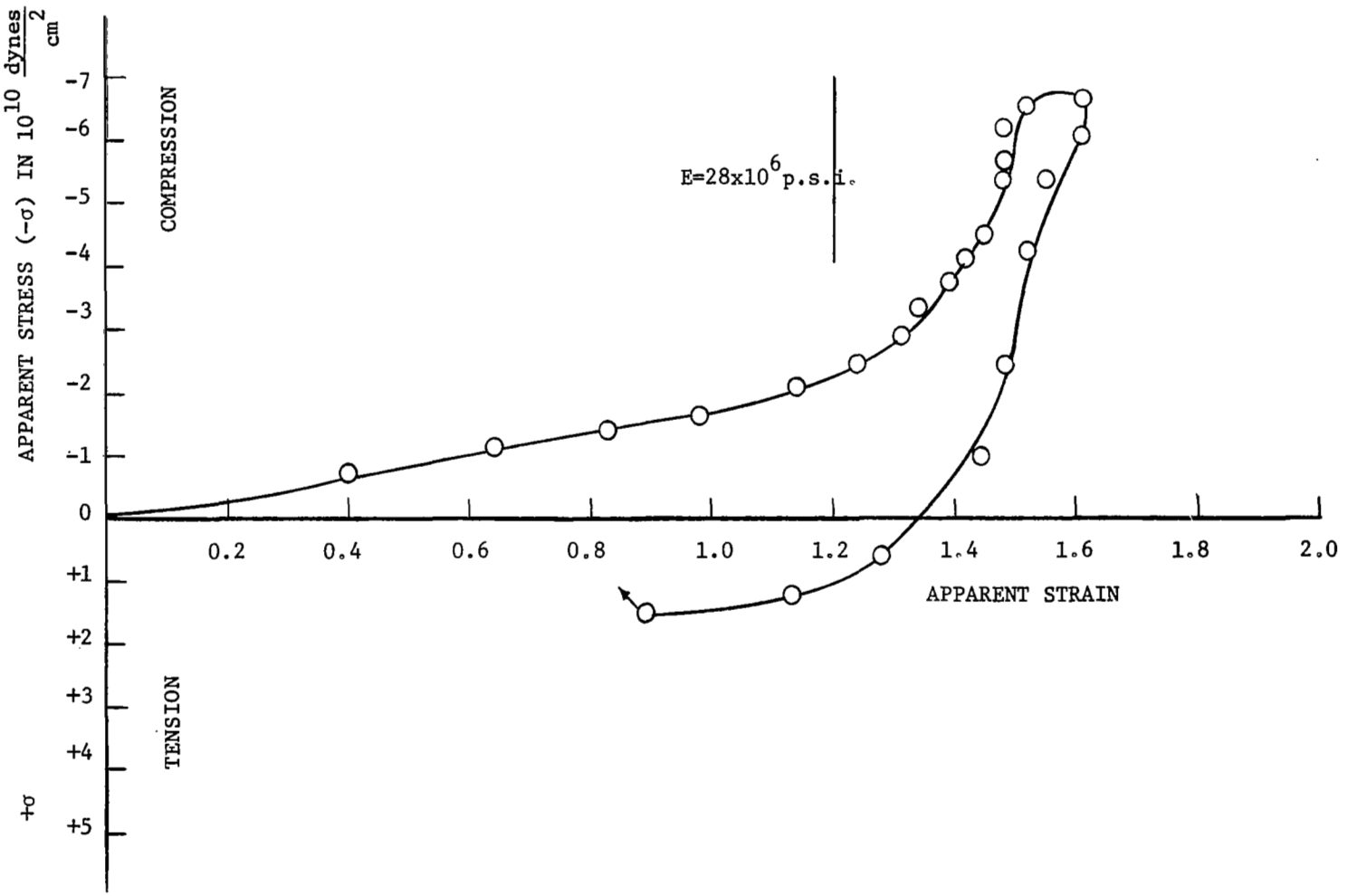

Figure 20: Static Adhesion Apparent Stress vs. Strain Diagram for Unclean Co-50Fe, in U.H.V. and at Room Temperature.
Maximum load: 1.5 grams
Minimum resistance: 16.7 mΩ

and that the degassing performed was insufficient to bring the dislocation concentration low enough to foster a brittle fracture. Of course, the possibility of other defects aiding in a ductile fracture is not overruled. One ought to note that extremely brittle nature of Co-50Fe may also appear to cause the continuous fracture of the interface as the load is released. In the case of Fe-8 ppmC one would expect a very ductile fracture; however, in a very brittle material such as Fe-50Co one would suspect that the area could be decreased by micro brittle fractures of each individual asperity. This technique cannot sort out the two types.

If, on the other hand, the surfaces are subject to any degree of contamination in excess of a fraction of a monolayer, a new line of reasoning might have to be submitted. Since surface characterization to this fine a degree is well beyond the usefulness of constriction resistance measurements and the scope of this investigation, detailed conclusions of this sort would have to remain until more elaborate experiments are performed.

The fact that thermal degassing alone of this alloy system produced contact resistance vs. load data which is quite similar to that of ultra clean iron[14] (argon ion cleaned) was somewhat surprising. Firstly, the contact resistance at a load of 1.3 grams was about 18 milliohms; and one would expect with the presence of an oxide, i.e. before argon ion cleaning, a resistance value in excess of 50 milliohms. Secondly, the overall slope of the Co-50Fe curve is quite similar to that of ultra clean iron[14] and the cleaned Co-50Fe samples presented later. A possible explanation is as follows: the temperature of degassing being about 900°C, the following reactions occur:

Reaction	Free Energy at 900°C K.cal/mole.	
$2\ Co + O_2 = 2\ CoO$	-70	
$2\ Fe + O_2 = 2\ FeO$	-90	
$4\ Fe + 3\ O_2 = 2\ Fe_2O_3$	-240	(18)
$6\ Fe + 4\ O_2 = 2\ Fe_3O_4$	-350	

Thus from the standard free energy of formation of oxides as a function of temperature[42], it is clear that at the temperature of degassing, only the oxides of Fe are stable and that CoO is reduced to the metallic state because the free energy of formation of CoO is greater (more positive) than that of any oxide of Fe. The following reaction could be predicted:

$$CoO + Fe \rightarrow Fe_xO_y + Co \qquad (19)$$

The oxides thus formed must in turn be either diffused into the Co-50Fe lattice or covered with cobalt since the contact resistance observed is that which would be predicted for ultra clean metal. Since oxygen does not appear to be at the surface and it was present before the experiment (exposure to atmosphere), it must have diffused into the lattice combining with the iron and leaving cobalt at the surface. The surface tension of Co and Fe are nearly idenetical; thus a preferential surface concentration of either cannot be predicted.

The oxide consideration just developed is one possibility, and a second could be based on the fact that the oxide is electronically conductive and plastic in nature as is the film which is formed by chemisorbed hydrogen on iron.[14] The argon ion cleaning of these samples and a comparative analysis

should eliminate one of the possibilities.

The estimated friction behavior of these materials is based on an analysis developed by McFarlane and Tabor[43] which suggested that interfacial strain and the coefficient of friction are closely related. Comparing the condition for plastic equilibrium in the contact area (as proposed by McFarlane and Tabor) with the apparent compressive interfacial strain as developed by Keller and Tsai[44]

$$1 + \alpha\mu^2 = \left(\frac{A}{A_o}\right)^2 \tag{20}$$

where α = a constant with values between 3 and 11 and μ = coefficient of friction.

Since

$$\varepsilon = 2 \ln \frac{R_o}{R_o^o} \tag{21}$$

then we may write:

$$\varepsilon = 1/2 \ln (1 + \alpha\mu^2) \tag{22}$$

Figure 21 depicts this relationship and clearly indicates that as strain developed in the contact region is increased, i.e. as the true area of metallic contact expands, the coefficient of friction will similarly be increased. Friction is thus defined in terms of the attractive forces developed across the interfacial zones constituting the true area supporting the load, and is consistent with previous models of friction[29]. In the case of metals, as we have discussed, these areas are measured and related to the friction process since only conductive areas are monitored.

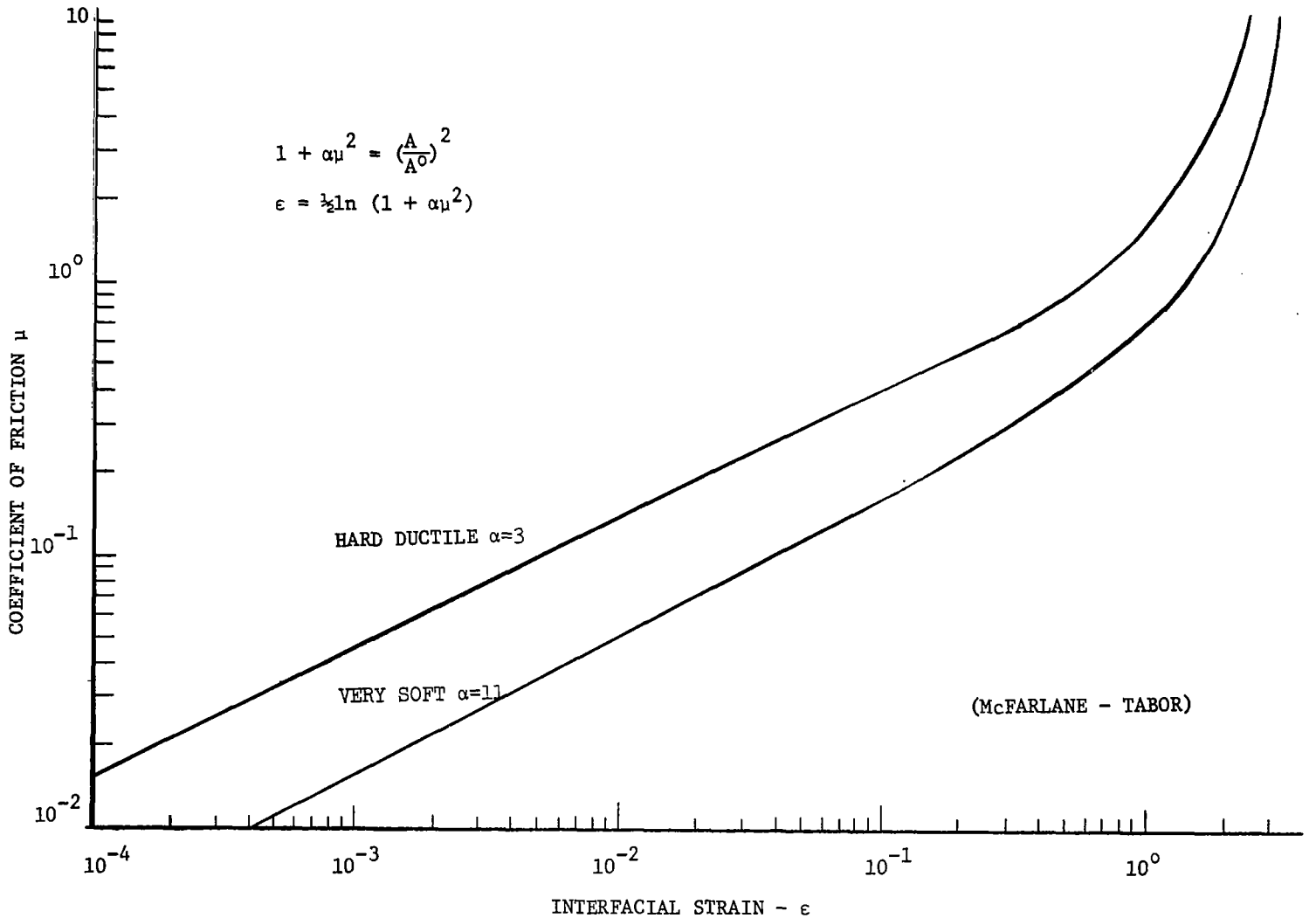

Figure 21: Variation of the Coefficient of Friction with Interfacial Strain.

For example, since the friction process involves a fracture process which is dependent on the applied or residual stresses as the load is released, one examines the load-release portion of the apparent stress-strain diagram at an appropriate operating stress level. The corresponding measured strain value is then inserted in Equation 22 (Figure 21) which is used to predict the value for the coefficient of friction. Using Buckley's configuration[46], for example, a Co-50Fe pin of 3/8 in. diameter loaded on a plate of similar material to 125 grams, would develop 71,100 p.s.i. contact stress (Hertz[45]). Under ultra high vacuum conditions of this experiment, these values (from Figures 19 and 20) correspond to about 1.00 and 1.41 strain units respectively, which from Figure 21 indicates coefficient of friction coefficient values in the ranges 0.74 to 1.42 and 1.16 to 2.22 respectively depending on the value of α* taken (11 or 3). This agrees fairly well with the same operating contact stress level, as 1.2 and 1.3 for the ordered and disordered structures of Co-50Fe respectively. A glance at Table 18 gives one an idea of the range in which the coefficient of friction (μ) lies (for α=11 and 3) for various surface conditions, and until a suitable value for α for this system is assumed, we could only say that the coefficient of friction is about 1.3±0.5. From the standpoint of adhesion, the Co-50Fe alloy does not seem to be a good bearing material as is evidenced by a fairly high coefficient of friction and from the fact that the interface withstands only a fraction of pressure release prior to fracture initiation and the remaining material providing

* The variable α established by McFarlane and Tabor has been more recently defined by Kragalski[47] as a function of stress concentration due to surface roughness.

some tensile strength. From the stand point of adhesion, a good bearing material should exhibit a condition in which nearly all of the elastic contact is recovered as the pressure is released. The above argument applies to all the remaining static adhesion apparent stress-strain curves presented in Figures 22-28 for Co-50 Fe.

A selected number of adhesion cycles under different surface conditions were reduced to apparent compressive stress-strain curves as illustrated in Figures 22-28 to illustrate the salient features of each condition. At least ten separate cycles for each of the conditions were examined and one or more of the most representative were included herein. One common feature for all surface conditions was that the fracture of the adhesion junctions were of the continuous type.

Code-1, Serial No. 1: Argon ion cleaned for six cycles of 15 minutes each. Adhesion run conducted in an argon atmosphere and room temperature. There was a time interval of three days between cleaning and experimentation, (Figure 22).

The apparent stress-strain curve in this case can be represented by a curve which extends to a point in excess of 100% strain to 135%. The slope of the loading portion of this curve at some point above 100% strain abruptly increases to a value in the range $1.90 \times 10^{12} \frac{\text{dynes}}{\text{cm}^2}$ which is about the value of the elastic modulus reported for Co-50 Fe (28×10^6 p.s.i.). The maximum slope of the curve as the load is released also approaches $1.90 \times 10^{12} \frac{\text{dynes}}{\text{cm}^2}$. The curve indicates regions of asperity collapse as well as regions in which the slope is the same as the elastic modulus of Co-50 Fe.

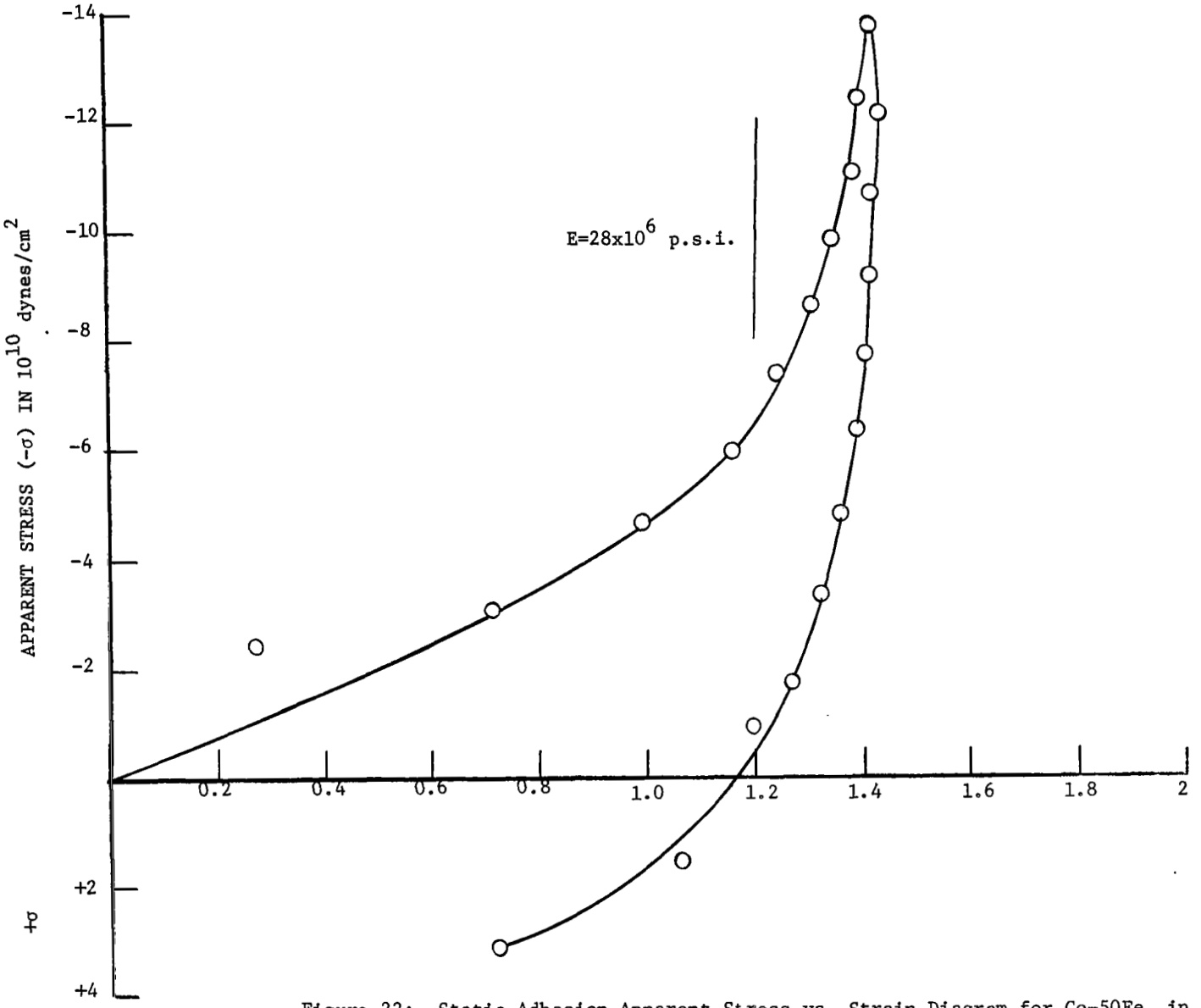

Figure 22: Static Adhesion Apparent Stress vs. Strain Diagram for Co-50Fe, in an Argon Atmosphere and at Room Temperature.
Maximum load: 0.9 grams
Minimum resistance: 31.3 mΩ

The interpretation of these curves follows along the analogy cited in the previous paragraphs (for the two adhesion runs after thermal degassing only) in which the initial contact involves few asperities and a large range of asperity collapse until the load can be supported elastically by the bulk system. The junction fracture of most of the tests in this case was by what is termed continuous as evidenced by the tensile portion of the curve in Figure 22. Since the test for this case was conducted in an argon atmosphere (after AIB), the $R_{o\ min.}$ value has increased from 18 mΩ in the case of thermal degassing alone, to about 31 mΩ. This could possibly be explained by the presence of adsorbed argon (most unlikely) or one could argue that the severe effects of argon ion bombardment similar to radiation damage, would develop a rather high concentration of defects at the contact point.

Referring to Figure 18 which shows three typical cases, A, B and C for the behavior of the apparent stress-strain curves after initiation of physical contact at zero stress-strain and as the load is increased, it is seen that the curves in Figures 22 to 28 correspond to case B which illustrates a situation in which the interface withstands a fraction of pressure release prior to fracture initation and the remaining material providing some tensile strength. This is evidenced by a decrease in strain which exceeds that decrease rate predicted by Young's Modulus. This happens in the event the metallic contact area is fracture sensitive to the severe notches in the contact zone or contaminated with a brittle phase, and the build up of elastic stress as the load is released may become sufficient to permit a crack to propagate and thus reduce the real area of contact.

It is seen that the apparent stress-strain curve in Figure 22 is similar to those curves in Figures 19 and 20 in which the Co-50Fe samples were only thermally degassed and not argon ion cleaned (c.f. early portions of this section). There were two possible explanations given for the observations in Figures 19 and 20. One was that oxygen present on the surface of Co-50Fe must have diffused into the lattice combining with iron and leaving the cobalt at the surface, the preferential concentration of either being unpredictable. The second possible explanation was that the oxide is electronically conductive and plastic in nature, similar to the film formed by chemisorbed hydrogen on iron[14]. The latter possibility is eliminated after the experiments conducted after argon ion bombardment, where one could be fairly sure that no significant amount of film, save a fraction of a monolayer, would remain on the surface.

The coefficient of friction calculated on the basis of the data of McFarlane and Tabor[43] was found to be in the range of 0.95 to 1.81 for α values of 11 and 3 respectively.

Code C-5, Serial No. 8: Argon ion cleaned for eight cycles of 15 minutes each. Thereafter annealed (1 cycle) at about 900°C for 30 minutes. Adhesion test conducted in UHV and at room temperature. Figure 23.

Tsai[14] observed that without exception, the second contact cycle, or third or fourth, etc. on the same contact spot in which the data of initial contact was obtained, developed an apparent stress-strain curve which was significantly displaced to a lower strain value. The apparent stress-strain curve in Figure 23 has a maximum strain of only 100% and the break to a steeper slope occurs around 60% strain. This curve and the apparent stress-strain curve in

Figure 25 are the only ones which have the initial slope somewhat larger than all the other curves presented for this system, though the apparent stress-strain curve in Figure 25 has a maximum strain of about 170% (the curve in Figure 25 will be discussed separately). This larger initial slope was also observed by Tsai[14] for multiple contacts, e.g. the same contact area contacted several times in succession. Figure 23 is definitely not the data obtained for initial contact and it is not possible to say whether it depicts the second or third etc. contact cycle, as these details were not noted.

The slope of the curve around 80% to 90% strain is about $4.2 \times 10^{10} \frac{\text{dynes}}{\text{cm}^2}$ which is one to two magnitudes less than the Elastic Modulus for the material ($190 \times 10^{10} \frac{\text{dynes}}{\text{cm}^2}$), whereas it approaches the Elastic Modulus during unloading.

The coefficient of friction in this case is in the range 0.57 to 1.10 depending on whether α = 11 or 3. This lower range of μ is to be expected because of the low strains developed within the material.

Code C-6, Serial No. 13: AIB 8 cycles at 15 minutes each, anneal 1 cycle of 30 minutes. Adhesion test conducted a day later at UHV and at room temperature. Figure 24.

The conditions during this test were nearly the same as the previous one except that a day had elapsed between annealing and the experiment. The maximum strain is about the same (105%), but the initial slope is less than that in Figure 23. Another difference is that the break to a steeper slope is around 85% strain and the slope approaches the Elastic Modulus near the maximum load (2.0 grams). On unloading, the slope again approaches the

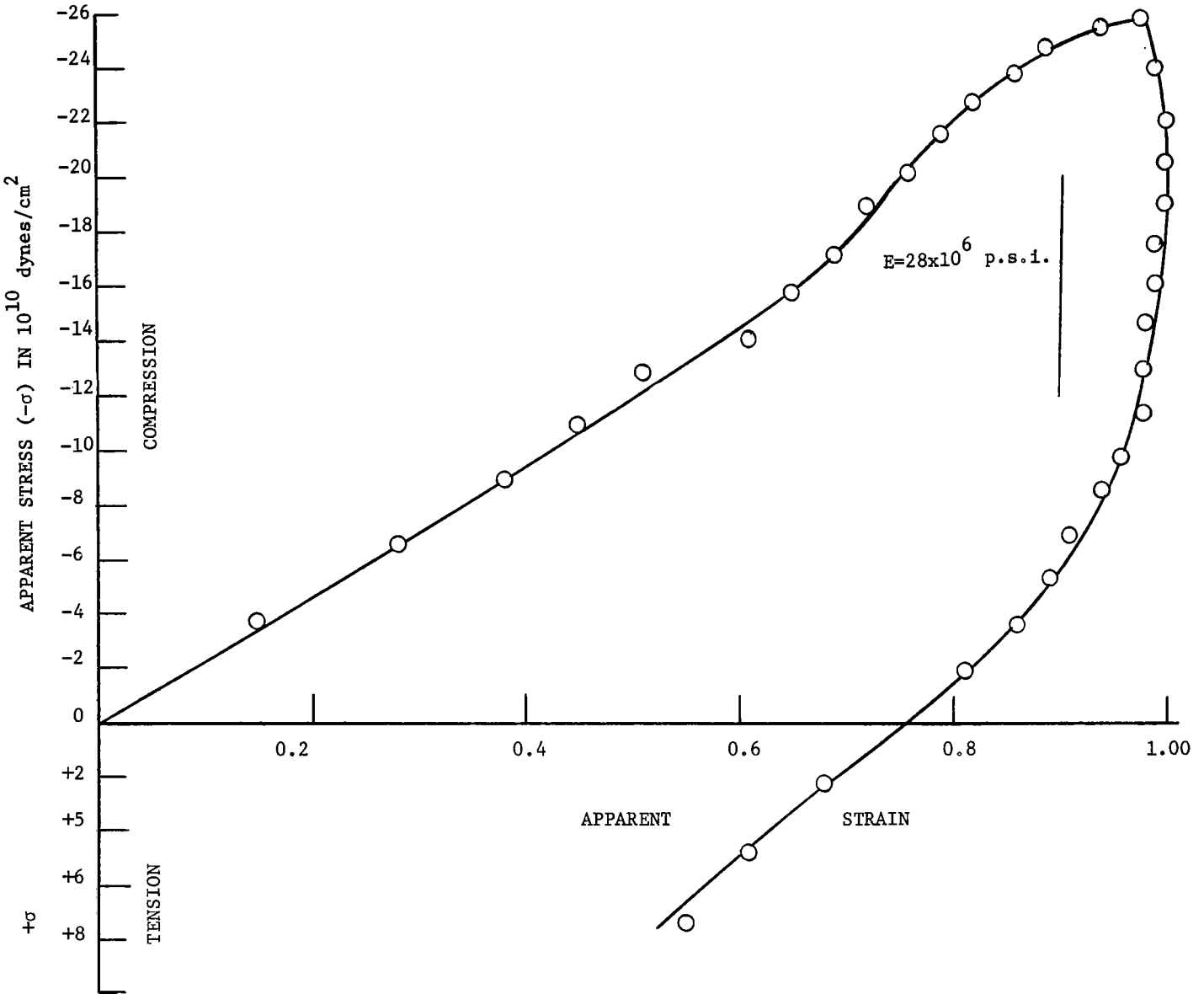

Figure 23: Static Adhesion Apparent Stress vs. Strain Diagram for Co-50Fe in UHV and at Room Temperature.
Maximum load: 1.6 grams, Minimum resistance: 32.7mΩ

Elastic Modulus and it looks as though the interface withstands only a small fraction of pressure release prior to fracture initiation and the remaining material providing a good amount of tensile strength. In fact, it somewhat approaches the case that on pressure release, the real contact area changes only by the variation due to elastic recovery. This is a case (and so is the one in Figure 25) which lies somewhere between the two above mentioned modes of behavior of the interface during unloading.

As expected, the coefficient of friction is quite low (0.72 to 1.35) because of the relatively low interfacial strains involved.

Code C-7, Serial No. 16: AIB 8 cycles of 15 minutes each, anneal 1 cycle (30 minutes) and AIB 1 cycle of 15 minutes. Adhesion test conducted in an argon atmosphere and at room temperature. Figure 25.

As already mentioned the initial slope of this curve is similar to that in Figure 23, the break to a steeper slope occuring around 90% strain and the slope as the maximum load (2.2 grams) approaches is around 2×10^{10} dynes/cm^2, which is about two magnitudes less than the Elastic Modulus. One essential difference from the curve in Figure 23 is that the maximum strain is about 170% which seems quite high for a multi-contact adhesion run. However, the conditions during this adhesion test were different, i.e. the test was conducted in an atmosphere of argon, immediately after AIB. For the same conditions, Tsai[14] observed, on an average, a shift of about 10%-20% in the higher strain direction, which he neglected in the light of scatter of data. For this metallic system, however, adsorbed argon has produced a significant shift of about 60-70% from the multi-contact adhesion run shown in Figure 23.

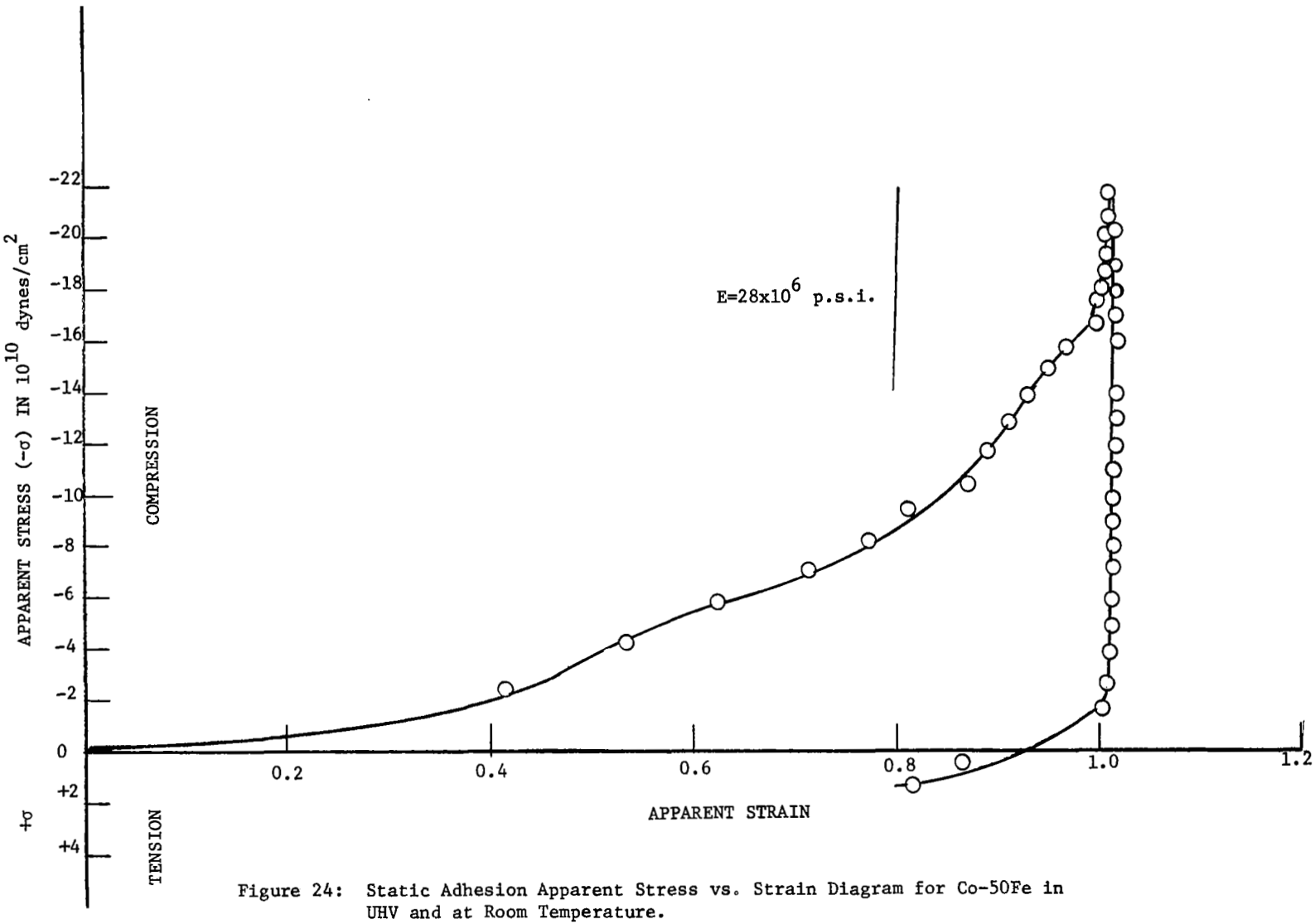

Figure 24: Static Adhesion Apparent Stress vs. Strain Diagram for Co-50Fe in UHV and at Room Temperature.
Maximum load: 2.0 grams
Minimum resistance: 26.5 mΩ

The curve on unloading has a similar behavior to that of Figure 24 and the same argument given for that, holds good. The coefficient of friction is in the range 1.54 to 2.94 and is slightly on the higher side when compared to 1.3 ± 0.5, due to the high interfacial strains involved.

Code C-8, Serial No. 20: AIB 8 cycles, anneal 2 cycles, AIB 1 cycle and anneal 1 cycle. Test conducted in UHV and at room temperature. Figure 26.

The break to a steeper slope is around 160% strain, the maximum strain being 200%. The slope approaches the Elastic Modulus around 175% to 185% strain and thereafter, on unloading, the slope reduces considerably to $2 \times 10^{10} \frac{\text{dynes}}{\text{cm}^2}$ which is about two magnitudes less than the Elastic Modulus of $190 \times 10^{10} \frac{\text{dynes}}{\text{cm}^2}$. On unloading, the behavior of the interface shows that it withstands a considerably large fraction of pressure release prior to fracture initiation, the remaining material providing a small amount of tensile strength.

For a maximum load of 1.8 grams, the lowest value of contact resistance measured was 15.5 mΩ which is the lowest measured so far. The contact resistance values for the adhesion runs in Figures (27 and 28) are also low and in proportion to the maximum load applied. The alternate cleaning treatments (AIB and annealing) has produced a nearly ultra clean surface as evidenced by the low value of contact resistance.

The coefficient of friction was found to be in the range of 0.99 to 1.89 which agrees fairly well with the value 1.3 ± 0.5.

Code C-8, Serial No. 21: Adhesion test conducted under the same conditions as the previous case. Figure 27.

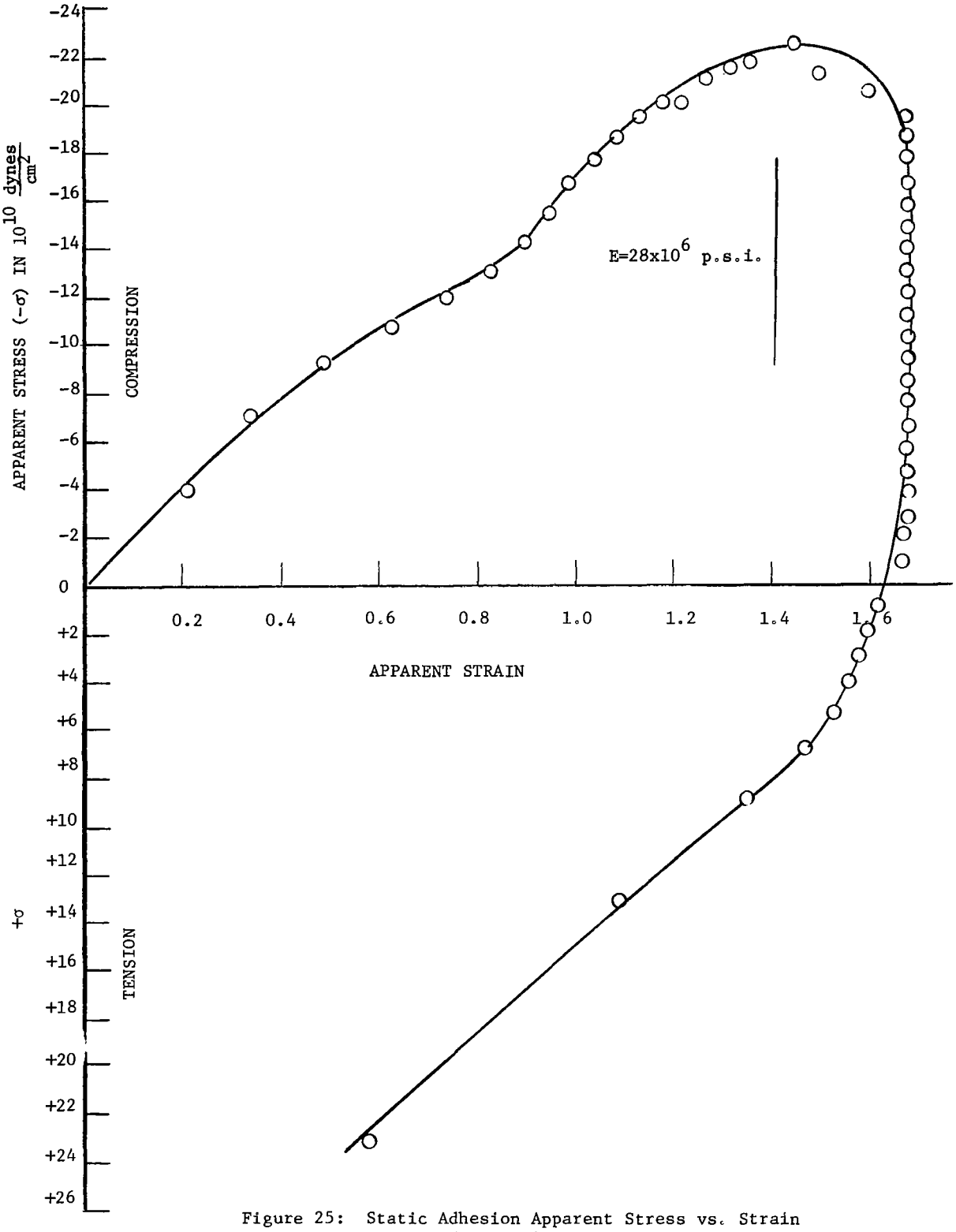

Figure 25: Static Adhesion Apparent Stress vs. Strain Diagram for Co-50Fe, in an Argon Atmosphere and at Room Temperature.
Maximum load: 2.2 grams, Minimum resistance: 25mΩ.

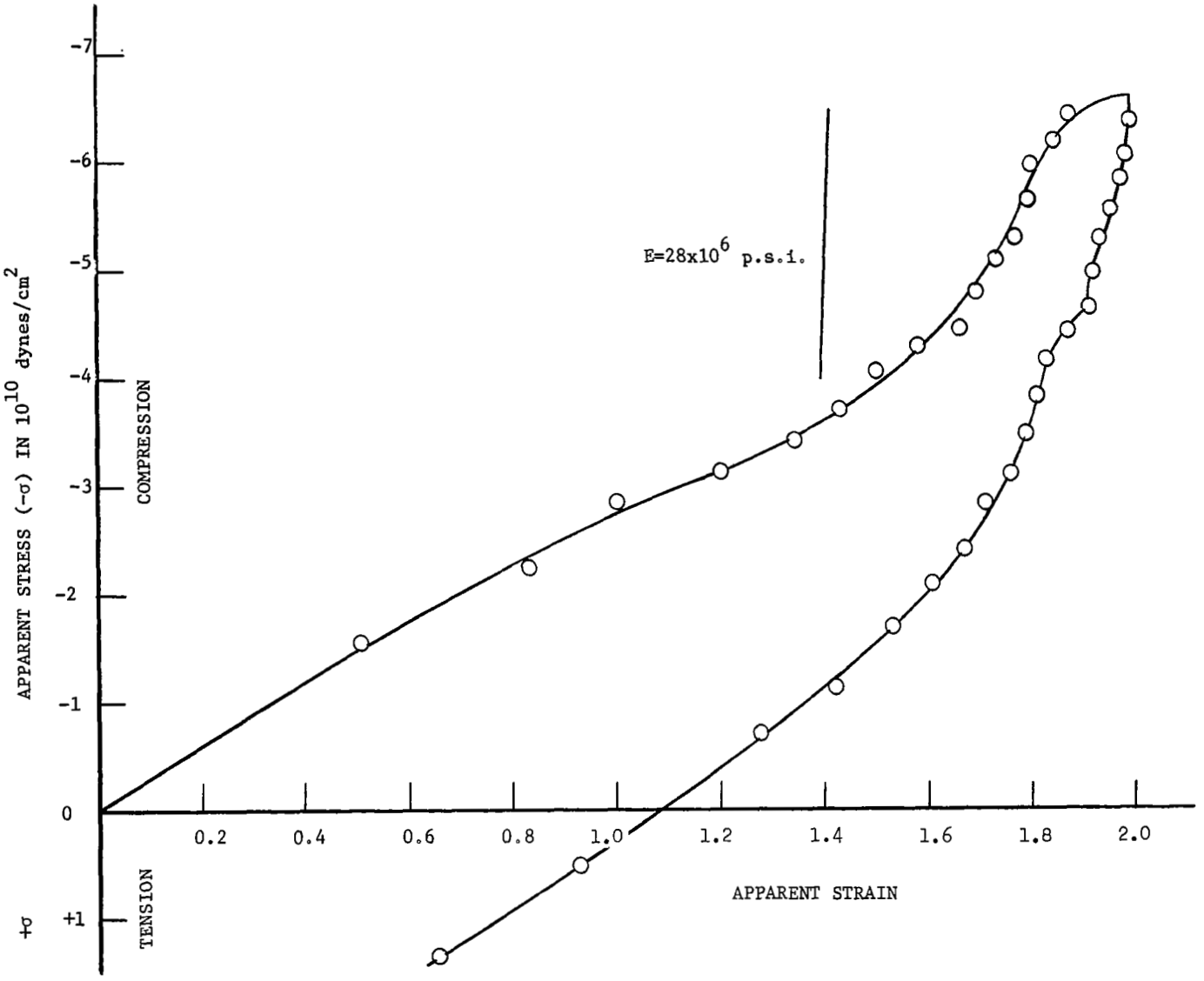

Figure 26: Static Adhesion Apparent Stress vs. Strain Diagram for Co-50Fe, in UHV and at Room Temperature.
Maximum load: 1.8 grams, Minimum resistance: 15.5 mΩ

The maximum load being less (1.5 grams) in this case, the maximum strain observed was around 165%. The break to a steeper slope is around 110% strain and the slope approaches the Elastic Modulus in certain portions as the maximum load is approached. The slope on unloading is around $10 \times 10^{10} \frac{\text{dynes}}{\text{cm}^2}$ which is more than a magnitude less than the Elastic Modulus of $190 \times 10^{10} \frac{\text{dynes}}{\text{cm}^2}$. Otherwise, the behavior of the interface on pressure release is almost identical to the previous case. The coefficient of friction is in the range of 0.80 to 1.53 which agrees well with 1.3 ± 0.5.

Code C-8, Serial No. 22: Adhesion test under the same conditions as the previous case. Figure 28.

The maximum strain observed was around 200% and the break to a steeper slope around 150% strain. The slope approaches the Elastic Modulus around 185% to 195% strain, and on unloading, certain portions of the curve have a slope of $2 \times 10^{10} \frac{\text{dynes}}{\text{cm}^2}$ which is about two magnitudes less than the Elastic Modulus. The behavior of the interface on unloading approaches more closely to adhesion run C-8, Serial No. 20 (Figure 26) and suggests that it withstands a great fraction of pressure release prior to fracture initiation, which is evidenced by a decrease in strain in which exceeds (by a great deal) that decrease rate predicted by Young's Modulus. In fact, it lies somewhere between cases B and C in Figure (18), leaning more towards Case C which characterizes an interface in which nearly all of the elastic contact is recovered as the pressure is released.

The coefficient of friction is in the range 0.96 to 1.83 which agrees well with 1.3 ± 0.5.

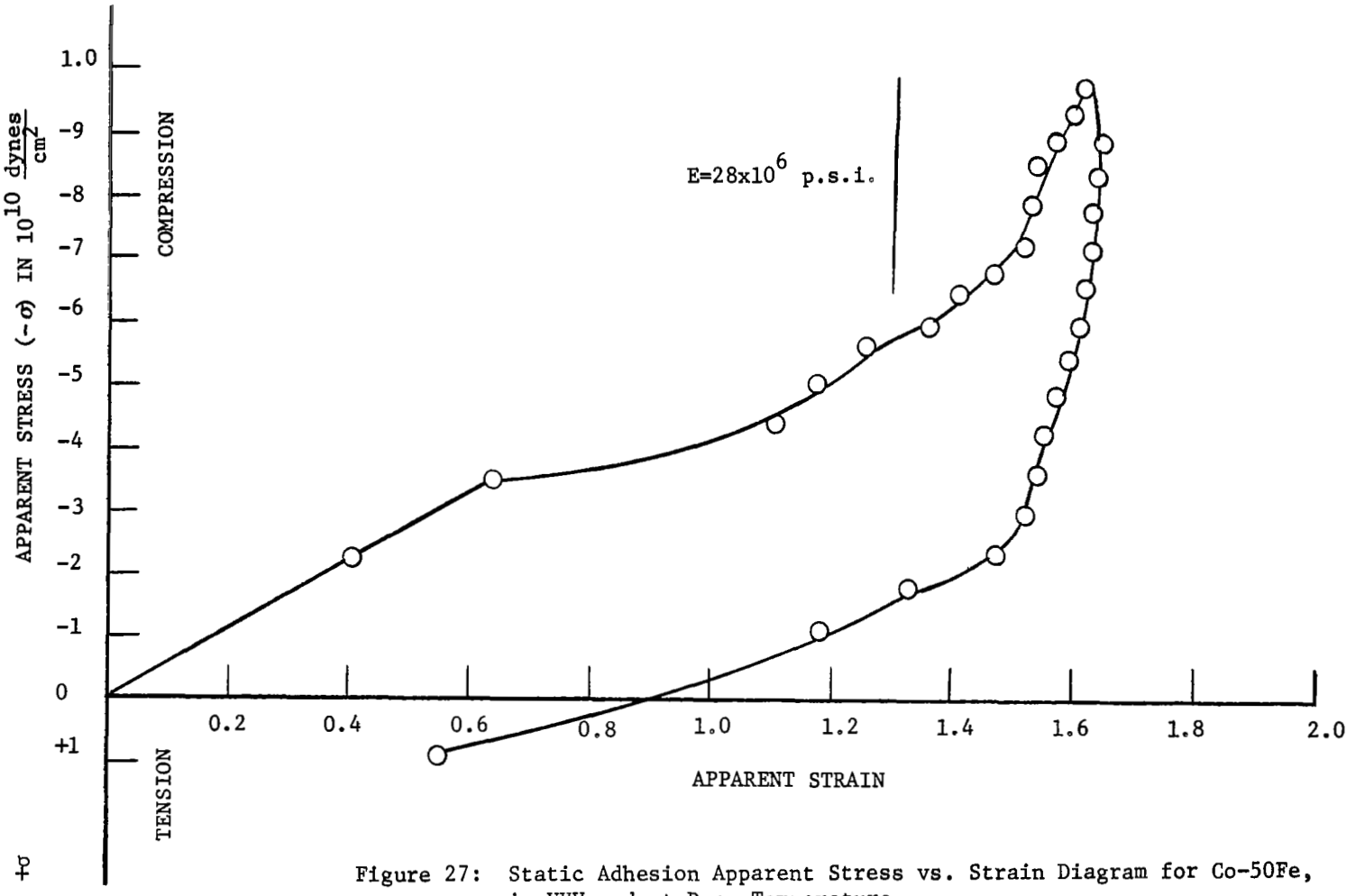

Figure 27: Static Adhesion Apparent Stress vs. Strain Diagram for Co-50Fe, in UHV and at Room Temperature.
Maximum load: 1.5 grams
Minimum resistance: 20.6 mΩ

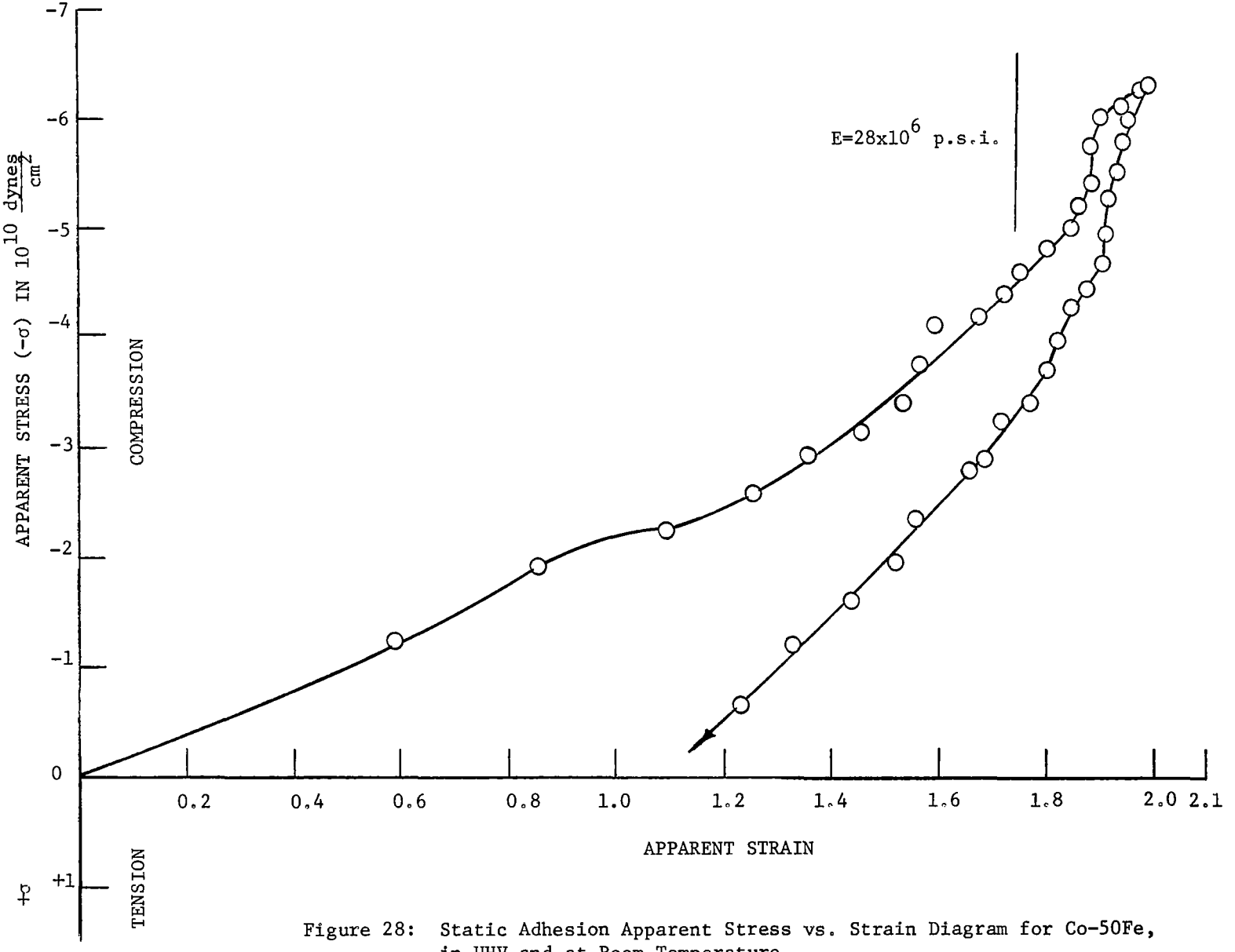

Figure 28: Static Adhesion Apparent Stress vs. Strain Diagram for Co-50Fe, in UHV and at Room Temperature.
Maximum load: 2.1 grams, Minimum resistance: 14.2 mΩ

Discussion on adhesion tests conducted on Cobalt - 25% Molybdenum - 10% Chromium alloy.

Chung conducted the static adhesion experiments on Co-25 Mo-10Cr cross rods and presented the static adhesion apparent stress-strain diagram (Figure 29) for ultra clean surfaces in UHV (1×10^{-9} Torr) and loaded to 2.5 grams. The test was conducted after repeated cycles of argon ion bombardment (12 cycles) and annealing till the contact resistance at a load of 2.5 grams was 28 mΩ. The first few cycles of surface cleaning produced a contact resistance value as high as 120 mΩ at the same load.

From the trace of the original adhesion test showing the observed contact resistance versus load, it was observed that the welded junction would have separated by a ductile fracture because the contact resistance increases slowly, i.e. contact area decreases as the tensile region is reached, which is characteristic of a ductile fracture. The explanation given in the previous section for Co-50Fe is valid in this case too.

In Figure (29), we see that the break to a steeper slope occurs around 25% strain, the maximum strain being only 60%. The slope around 50% to 60% strain is 5.05×10^{6} p.s.i. which is about six times lower than the Elastic Modulus for the material (30×10^{6} p.s.i.). On unloading, at the first instant, the slope approaches the value of the Elastic Modulus and thereafter drops to a magnitude less than the Modulus.

Comparing Figure (29) to Figure (18) we see that the interface (junction) behavior resembles the extreme situation in which nearly all of the elastic contact is recovered, as the pressure is released. This case is representative of a good bearing material from the standpoint of adhesion, quite unlike the

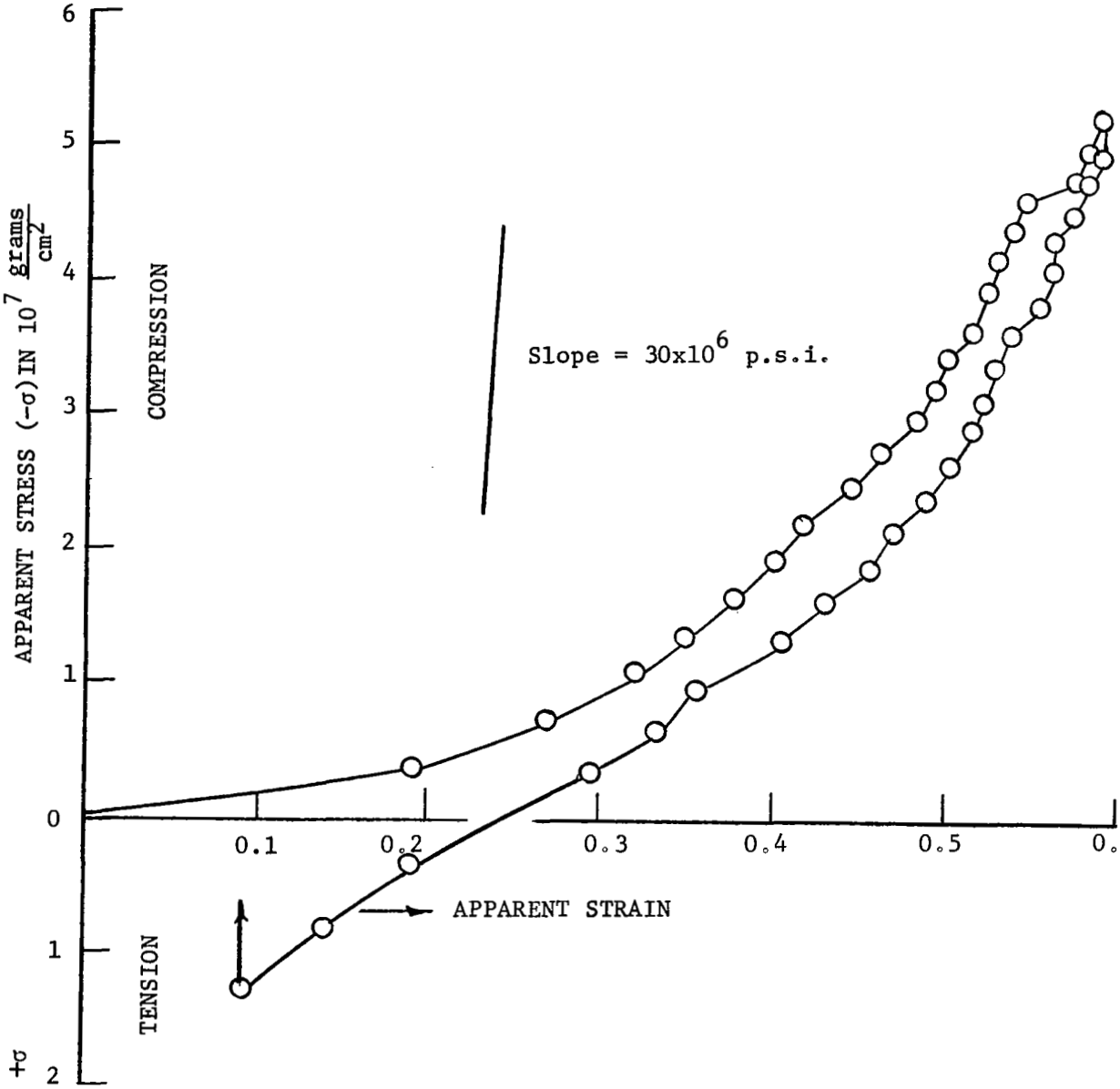

Figure 29: Static Adhesion Apparent Stress-Strain Diagram for Co-25Mo-10 Cr. Ultra Clean Surfacesin UHV Loaded to 2.5 grams.

Co-50Fe alloy whose interface (in most cases) withstood only a fraction of pressure release prior to fracture initiation of the welded junction.

Another striking difference between the static adhesion apparent stress-strain curves of Co-50Fe and Co-25 Mo-10Cr is that the maximum strain in the latter is only around 60%. One would therefore expect a relatively lower value for the coefficient of friction. Just as in the previous case, if the estimated friction behavior is based on McFarlane and Tabor's[43] data (with suitable choice of an operating contact stress level), the friction coefficient is found to be in the range of 0.29 to 0.55 depending whether the value of α chosen was 11 or 3. (c.f. previous sections). This value is consistent with expectation (for Co-50Fe it was 1.3 ± 0.5) and agrees with that found by Brainard[48] for the same system and the same operating contact stress level. The dynamic coefficient of friction value found by Buckley for this alloy was 0.25 which can be considered as an excellent agreement considering the various approximations necessary in obtaining the predicted value.

Discussion on surface cleaning

Since cleaning of the metal surfaces was done by using ion bombardment and annealing as a method, certain criteria have to be considered before making any rash conclusions about the cleanness of the so-called 'ultra clean surface'. Farnsworth[49, 50] discusses some of the drawbacks when using the above method of cleaning.

(a) Boron contamination, which originates from the Pyrex surfaces are transferred by water vapor and therefore ion bombardment should be applied after bakeout and before high temperature annealing. For the Co-50Fe experiments, the adhesion cell was an all metal system and hence this drawback

eliminated; but for the Co-25Mo-10Cr, the investigation was conducted in a pyrex adhesion cell and thus boron contamination may be expected as water vapor is present in any UHV system of even 10^{-10} Torr.

(b) Stable chemical compounds are, or can be formed on the surface. For instance, boron cannot be removed by annealing if its melting point is higher than the annealing temperature.

(c) When a metal is heated after ion bombardment, bulk impurities may diffuse onto the surface, and cannot be removed by heating below their melting point.

(d) Diffusion of surface impurities to a thin underlayer, thus allowing the surface to appear clean, yet contamination is below the surface. This could effect the adhesion of the "clean" interface with an altered contact resistance value, especially at the maximum load.

Kaminsky[51] has pointed out the structural changes in pure metals or alloys as a result of ion bombardment, on the basis of investigations by several authors. When a binary alloy is bombarded with positive ions of an inert gas, in many instances one of the metals is initially removed more rapidly than the other. Consequently, a thin layer of alloy of a new and uniform composition is formed on the surface. Asada et al.[52] found that ion bombardment of Cu alloyed with very small amounts of Au, sputtered the gold faster than the copper so that the surface was enriched in copper. When Cu_3Au alloys were bombarded with Ar^+ ions at energies up to 5 kev, however, Ogiluie[53] observed that the copper is removed more readily than gold. Since the ratio of sputtered Cu to sputtered Au atoms is more than 3:1, the surface layers become enriched in gold. Fisher et al.[54] observed

that when the alloy consisting of 70% brass, 30% stainless steel was sputtered by Krypton ions, the sputtered material had the same composition as the original alloy. Hanau[55] found similar results for aluminum alloys.

Residual gases are usually present in small low pressure systems. For a glass and metal system using an oil diffusion pump. Singleton[56] found the main residual gas components to be CO_2, CO and H_2. These, along with the impurities (O_2, N_2, H_2O, hydrocarbons, CO_2 and H_2 which totally are <7 p.p.m.) present in the research grade Argon used for ion bombardment, could easily contaminate a newly cleaned surface. For example, to form one monolayer of a gas (say, H_2) on a metal surface, at a system pressure of 10^{-9} Torr, it takes about 1000 seconds.

It is difficult to say anything quantitative about the state of cleanness of the metal surface, taking into considering the presence of residual gases and the possibility of diffusion of impurities (both surface and bulk) after ion bombardment and anneal. As regards preferential sputtering in the alloy systems investigated, nothing can be said at present.

Discussion on the correlation of metallurgical structure and properties on the adhesion and friction behavior.

I. Cobalt - 50% Iron: The mechanical properties of the disordered and brittle alloy indicated an exceedingly low fracture strength, low hardness and very weak grain boundary strength. Ordering by suitable heat treatment only produced a more brittle material with a lower fracture strength and a slightly higher hardness value. It was not possible to make adhesion samples from the alloy in either of the above states due to mechanical failure during wet grinding. Work

hardening was found to produce a finer grain structure and a greater grain boundary strength which was amenable to the grinding such that adhesion samples could be formed. Irrespective of the heat treatment given the alloy before mounting into the adhesion apparatus, the extensive ultra high vacuum thermal degassing at 900°C to clean the specimen surface such as was used in these experiments resulted in only an annealed alloy for the adhesion testing. One should note, however, that the extensive high temperature degassing can be avoided, if heat treated specimens are to be tested as was cited by Aldrich and Keller[15].

One should not make the error of interpreting the static adhesion apparent stress-strain curves in the same manner as the typical engineering stress-strain curve due to the assumptions necessary for their development. For example, the calculated fracture stress of the cobalt-iron alloy for the numerous adhesion tests showed values in the range of 80 k.s.i. to 150 k.s.i. (some cases even 1000 k.s.i.) depending on conditions of the experiment whereas the bulk strength of the alloy was observed to be about 10 times less than these values.

The greater fracture strength calculated from the adhesion data were due apparently to our inability to place the stress values on an absolute scale. On the other hand, the observed adhesion strengths may in fact be truly representative of the bulk strength of the crystal and the observed bulk strength values were low due to the weak grain boundaries. Under the present circumstances there is no way to clarify this situation since alloy single crystals cannot be made available and absolute area identification is most difficult. Both of these aspects were beyond the scope of this program.

The Co-50Fe alloy which is comparatively soft but highly brittle, when subjected to adhesion tests, exhibited what was called "ductile", fracture (on load release), i.e. the contact junction upon release of the compressive load decreased in area in a continuous manner. In the light of the mechanical properties of this alloy it is reasonable to assume that the asperity collapse upon load application is not simply plastic in nature, but that they crumble due to the highly brittle nature of the alloy, c.f. scratch by silicon carbide in Figure 4. The strengths of the adhesion junctions were somewhat higher than anticipated and the fracture stress values showed a higher degree of scatter than those for pure iron. On load release the various welded junctions at the contacting interface fractured in a brittle manner, asperity at a time, thereby giving an overall appearance of what appeared to be a continuous process as was observed in some of the cases for iron. The wear track of the dynamic friction tests were deep and appeared as though considerable material was "chipped" away which also supports this model.

The Co-50Fe alloy being soft and having a b.c.c. structure, one would expect high adhesion strengths and consequently a high friction coefficient, e.g. five to six; however, due to the reasons mentioned above the dynamic friction coefficient was only 1.3 ± 0.5 instead of the expected higher values as attained for pure b.c.c. iron[57]. The peculiar behavior of the Co-50Fe alloy is not fully explainable. The brittle nature of this material is due in some part to the weak grain boundaries and certainly the porosity also contributes to the lack of strength; however, each of these, or their combination, would not account for the low hardness nor the excessive wear evidenced in the dynamic friction

tests. The properties, which are quite similar to those of bismuth or graphite, suggest a low cohesive energy possible in one or more crystallographic directions coupled with a high need for atomic bond directionality. The basic problem is that Co-50Fe would not generally be considered to have such spectacular properties in the light of a phase stability analysis such as that provided by the Brewer-Engle[58] or Goodenough[59] theories. There is a distinct similarity between the mechanical properties of Co-50Fe and the γ-brass in the copper zinc-system.

The vacuum coefficient of friction at the operating contact stress level was 1.3 ± 0.5 which is much greater than that measured for most metals in air ($\mu = 0.1$ to 0.2). It has therefore been confirmed that due to the low rate of accumulation of gas on an exposed surface in UHV there are observable effects in several mechanical properties. In particular, compared to the properties in the atmosphere:

(i) Large increases in the adhesive forces between the surfaces brought into contact.

(ii) Friction coefficients of contacting bodies has also increased.

(iii) Observable changes have occured in ductility and resistance to fracture.

II. Cobalt - 25 Molybdenum - 10 Chromium: The observable effects or changes in the contact properties due to clean surface in UHV as mentioned above is applicable in this case too. For example, the fracture strength (after adhesion tests) is around 180 k.s.i. which is about five times more than the values observed from the engineering stress-strain curve. Also, the fracture

mode of the adhesion junction was much like that of Fe-50Co whereas it was brittle during the standard tension tests. The high hardness of the alloy (Rockwell-50) and its composite crystal structure (two of the phases being hexagonal and the third being rhombohedral) would permit the prediction a low adhesion strength; and consequently, a low value of friction coefficient[60] A value of 0.29 to 0.55 dynamic coefficient of friction confirms these expectations.

Co-25 Mo-10 Cr alloy, though brittle, has a high fracture strength as evidenced by the engineering tension tests. The lower junction strength from the adhesion tests, could be due to the composite structure (as just mentioned) of the alloy, and could also be due to the presence of surface contaminants. A re-examination of this alloy in the adhesion apparatus would characterize the interface behavior more clearly. These studies are in progress.

CONCLUSIONS AND RECOMMENDATIONS

I. Cobalt - 50 Iron

1. The contact behavior of Co-50Fe was characterized, and from these data we concluded:
   (a) Lower than anticipated adhesion strength for a b.c.c. alloy and hence a lower friction coefficient, but relative to Co-25Mo-10Cr the value is quite high.
   (b) The alloy is very brittle and structurally weak in all conditions, i.e. 'as-cast' (disordered), ordered and solution treatment.
2. The mechanical properties of the Co-50Fe alloy in the disordered state did not vary significantly from that of the ordered. A small increase in hardness was observed. Tension tests in the ordered state were barely possible due to a considerable increase in brittleness.
3. The present investigation confirmed the formation of a superlattice structure (type B2) in Co-50Fe at a temperature of about 730°C. The ordering was characterized by three extra diffraction peaks whose (hkl) indices are given by (100), (111) and (210).
4. A thorough investigation of the ordering transformation and the grain boundary strengths in this alloy would throw more light on the peculiar mechanical behavior of this alloy.

II. Cobalt-25 Molybdenum-10 Chromium

1. On the basis of contact behavior characterization, Co-25 Mo-10Cr

is a good bearing alloy i.e. from the standpoint of adhesion. It has low adhesion strength and demonstrates a low coefficient of friction.

(2) Co-25 Mo-10Cr being a brittle material and also very hard which does not permit simple forming.

(3) None of the heat treatments such as solution treating, annealing at 1220°C nor aging at 700°C and 800°C produced any significant change in the mechanical properties of the alloy.

(4) It is recommended that an alloy of Co-Mo-Cr of a 22 w/o Mo content with a larger α-phase field be made available for better solution treatment and thus permit proper precipitation hardening.

(5) Hexagonal metal systems which have abnormally low friction coefficients should be subjected to this broad based general study in which all material properties could be investigated in conjunction with metallic adhesion phenomena. The cobalt-rhenium system, which forms a series of hexagonal solid solutions could prove to be a useful system.

Probably the greatest contribution of this work is the generation of static adhesion data which permits the prediction of a coefficient of dynamic friction. Two alloys of very different mechanical behavior were used to predict coefficient of friction values and these predictions confirmed by an outside agency to be within 20%. Such has not previously been accomplished.

It is recommended that a serious investigation of the constant α in the McFarlane-Tabor relationship be initiated. An expansion of this type of investigation should be made to other types of alloys.

APPENDIX I

X-RAY, TENSION TESTS AND HARDNESS DATA FOR COBALT-50 IRON AND COBALT-25 MOLYBDENUM-10 CHROMIUM ALLOYS

TABLE 1

PROPERTIES OF Co-50Fe ALLOY IN VARIOUS CONDITIONS

Property	As Cast (Disordered)	Annealed at $725\pm10^{\circ}C$ for 100 hours (ordered)
Fracture Stress p.s.i.	(1) 16,700* (2) 11,300 (3) 10,600** (4) 9,150*	(1) Fractured while machining (2) 5,100 (3) 2,550***
Young's Modulus p.s.i.	(1) 33.4×10^6 (2) 22.6×10^6 (3) 21.2×10^6 (4) 18.3×10^6	--
Reduction in Area	NIL	NIL
Hardness Rockwell B (Average)	78	82

*Fracture outside of gauge length.

**Fracture at two regions, but within the gauge length.

***Fracture at two regions, one within and the other outside the gauge length.

NOTE: Hardness of work-hardened Co-50Fe alloy = 87 R_B (Average of 12 readings).
Hardness of work-hardened and then ordered (anneal at $725\pm5^{\circ}C$ for 100 hours) Co-50Fe alloy = 82 R_B (Average of 12 readings).

TABLE 2

SPECIMEN: Co-50Fe

TREATMENT: Aged at 710°C for 100 hours

RADIATION: Cr Kα

FILTER: Vanadium

Plane	Relative Intensity	d (A°)
(100)	5	2.86
(101)	100	2.05
(111)	5	1.645
(200)	20	1.425
(210)	5	1.275
(211)	30	1.165

TABLE 3

SPECIMEN: Co-50Fe (metallographic sample)

TREATMENT: Aged 725°C for 100 hours

RADIATION: Cr Kα

FILTER: Vanadium

Plane	Relative Intensity	d (A°)
(100)	2.0	2.68
(101)	100	2.02
(111)	2.0	1.65
(200)	31	1.42
(210)	4.1	1.28
(211)	81	1.16

TABLE 4

SPECIMEN: Co-50Fe Plate (Top Side with larger grains exposed to x-rays)

TREATMENT: Aged at 725°C for 100 hours (ordered)

RADIATION: Cr Kα

FILTER: Vanadium

Plane	Relative Intensity	d (A°)
(101)	100	2.04
(111)	0.5	1.66
(200)	1.0	1.43
(210)	0.7	1.28
(211)	2.5	1.16

TABLE 5

SPECIMEN: Co-50Fe (exposed on edge of plate)

TREATMENT: Aged at 725°C for 100 hours

RADIATION: Cr Kα

FILTER: Vanadium

Plane	Relative Intensity	d (A°)
(100)	5	2.65
(101)	100	2.09
(111)	1.1	1.64
(200)	1.7	1.50
(210)	2	1.28
(211)	100	1.16

TABLE 6

SPECIMEN: Co-50Fe (Bar)

TREATMENT: Work hardened at 1050°C (in γ region and furnace cooled)

RADIATION: Cr Kα

FILTER: Vanadium

Plane	Relative Intensity	d (A°)
(101)	100	2.01
(200)	9	1.43
(211)	24	1.16

TABLE 7

X-RAY DATA FROM Co-25Mo-10Cr ALLOYS

X-RAY PEAK INTENSITY

d Å	AS-CAST	SOLUTION TREATED	AGED 700°C	AGED 800°C	REMARKS
3.025	3				Co_3Mo
2.60	3				
2.389				80	μ Phase* 2.36 ms
2.384		100			
2.378			8		
2.365	4				
2.319			2		
2.301				4	μ Phase* 2.27 vw
2.296		5			
2.218			25		
2.214	10				
2.179+	4				μ Phase* 2.18 vw
2.177		20		40	
2.165			7		
2.138		11			ε - Cobalt (100) + μ Phase: 2.14* m
2.133				25	
2.126			5		
2.123					
2.085				100	ε - Cobalt (002) + μ Phase: 2.10* mw : 205* s
2.084		80			
2.069	20				
2.060		52(?)			

X-RAY PEAK INTENSITY

d Å	AS-CAST	SOLUTION TREATED	AGED 700°C	AGED 800°C	REMARKS
2.063				55	ε - Cobalt (002) + μ Phase: 2.10* mw : 205* s
2.054			58		
2.033				35	μ Phase: 2.03* mw : 1.99 mw
2.027			6		
2.021	5				
1.967		18			μ Phase: 1.94* m
1.964				17	
1.949	100		100		ε - Cobalt (101) + μ Phase: 1.91*
1.919		20			
1.918				21	
1.906	3				
1.852	3				μ Phase: 1.85* w
1.834		8			
1.830				10	
1.822			3		
1.809	3				?
1.801				8	
1.799+		8			
1.786	4				μ Phase: 1.77* w
1.782				2	
1.746				3	Some μ Phase lines have been reported as very weak
1.740		4			
1.599			1.5		
1.544			1.5		

X-RAY PEAK INTENSITY

d Å	AS-CAST	SOLUTION TREATED	AGED 700°C	AGED 800°C	REMARKS
1.504	37		16*	**	
1.491	3				Some μ Phase lines have been reported as very weak
1.481	2				
1.466			1.5		
1.403				4	cf. lines above 1.481
1.392	2				
1.376				17	
1.374		17			μ Phase: 1.38* vw
1.369+			1.5		1.36* m
1.367				6	
1.358	2				
1.332				23	
1.329		16			
1.328			3		μ Phase: 1.34* vw
1.309		30		35	1.32* ms
1.304	3		5		
1.296				25	
1.295		16			
1.277	13				ε-Cobalt (110)
1.276			16		
1.265				10	
1.261		5			
1.257	6				μ Phase: 1.27* mw
1.251			1.5		1.25 m
1.244			1.5		1.24 vw

X-RAY PEAK INTENSITY

d Å	AS-CAST	SOLUTION TREATED	AGED 700° C	AGED 800°C	REMARKS
1.241	2				μ Phase: 1.27* mw 1.25 m 1.24 vw
1.236		5			
1.233			1.5		
1.220				30	μ Phase: 1.22* vw 1.21 vs
1.218		14			
1.214			6		
1.211	2				
1.203			4		
1.191				73	ε Cobalt + μ Phase: 1.18* vs
1.189		55			
1.187			9		
1.180				8	
1.173				5	ε-Cobalt (103)
1.165				4	
1.162	87		46		
1.161				4	

* As given by B. Lux and W. Ballmann, Cobalt, 11, 4 (1961) which agrees well with S. P. Rideout and P. A. Beck, NACA Technical Report No. 1122 (1951).

TABLE 8

PROPERTIES OF Co-25Mo-10Cr ALLOY IN VARIOUS CONDITIONS

Properties	As-Cast	Annealing In Vacuum Furnace 1220°C-116 hours	Heat Treated Commercially 1200°C-60 hours	Aged 700°C-50 hours	Aged 800°C-61 hours (B)	Aged 800°C-61 hours (A)
Yield Stress p.s.i.	(1) 1.04×10^4 (2) 1.71×10^4	1.84×10^4	1.37×10^4	1.22×10^4	1.02×10^4	0.772×10^4
Fracture Stress p.s.i.	(1) 1.38×10^4* (2) 1.71×10^4*	3.42×10^4*	2.80×10^4	2.42×10^4	3.14×10^4	2.17×10^4*
Young's Modulus p.s.i.	(1) 17.4×10^6 (2) 24.4×10^6	108.6×10^6	$29\text{-}32 \times 10^6$	34×10^6	40.75×10^6	32.5×10^6
Reduction In Area	NIL	0.16%	Nil	0.16%	0.16%	0.16%
Hardness Rockwell C (Average)	49	49	47	51	52	50

"A" Aging done after annealing in vacuum at 1220°C for 116 hours.
"B" Aging done after commercial heat treatment at 1200°C for 60 hours and air cooled.
* Fracture outside of gauge length.

APPENDIX II

ADHESION DATA FOR COBALT-50 IRON COUPLES UNDER VARIOUS STATES OF CLEANNESS AND LOADS

TABLE 9

ADHESION RUN AFTER DEGAS (WITHOUT AIB)

	No.	Load w (grams)	Contact Resistance R_o (mΩ)	Apparent Stress σ (10^{10} dynes/cm^2)	Apparent Strain (ε)
	1	0.00	32.2=R_o^o	0	0
	2	0.025	29.6	-0.34	0.17
	3	0.05	27.9	-0.59	0.28
	4	0.10	25.6	-0.01	0.45
	5	0.15	24.6	-1.40	0.55
	6	0.23	22.9	-1.86	0.69
LOAD	7	0.35	21.9	-2.59	0.77
	8	0.47	21.2	-3.25	0.83
	9	0.60	20.9	-4.04	0.86
	10	0.85	20.2	-5.34	0.93
	11	0.97	19.9	-5.92	0.96
	12	1.10	19.6	-6.51	0.99
	13	1.33	18.9	-7.32	1.07
	14	1.10	18.9	-6.05	1.07
	15	0.97	18.9	-5.34	1.07
	16	0.85	18.98	-4.72	1.06
UN-	17	0.60	19.1	-3.37	1.06
LOAD	18	0.47	19.2	-2.67	1.04
	19	0.35	19.2	-1.99	1.04
	20	0.22	19.5	-1.29	1.01
	21	0.15	19.6	-0.89	1.00
	22	0.10	19.9	-0.61	1.00
	23	0.00	20.2	-	-
	24	-0.08	21.2	+0.55	0.84
	25	-0.12	24.6	+1.12	0.55
	26	-0.13	27.9	+1.56	0.28
	27	-0.14	31.2	+2.10	0.06

TABLE 10

ADHESION RUN AFTER DEGAS (WITHOUT AIB)

	No.	Load w (grams)	Contact Resistance R_o (mΩ)	Apparent Stress σ (10^{10} dynes/cm^2)	Apparent Strain (ε)
	1	0.00	$37.0=R_o^o$	0	0
	2	0.05	30.4	-0.71	0.40
	3	0.10	27.0	-1.12	0.64
	4	0.15	24.4	-1.38	0.83
	5	0.20	22.7	-1.59	0.98
	6	0.30	21.0	-2.04	1.14
	7	0.40	19.9	-2.44	1.24
	8	0.50	19.2	-2.84	1.31
LOAD	9	0.60	18.9	-3.30	1.34
	10	0.70	18.5	-3.69	1.39
	11	0.80	18.2	-4.08	1.42
	12	0.90	17.9	-4.44	1.45
	13	1.10	17.7	-5.31	1.48
	14	1.20	17.7	-5.79	1.48
	15	1.30	17.5	-6.13	1.48
	16	1.40	17.4	-6.53	1.52
	17	1.53	16.7	-6.57	1.61
	18	1.40	16.7	-6.01	1.61
	19	1.20	17.0	-5.34	1.55
UNLOAD	20	0.90	17.4	-6.20	1.52
	21	0.50	17.7	-2.41	1.48
	22	0.20	18.0	-0.99	1.44
	23	0.00	18.4		
	24	-0.1	19.7	+0.60	1.27
	25	-0.175	21.0	+1.19	1.13
	26	-0.175	23.7	+1.51	0.89
	27	-0.185	27.0	+2.08	0.63

TABLE 11

ADHESION RUN C-1, S-1

	No.	Load w (grams)	Contact Resistance R_o (mΩ)	Apparent Stress σ (10^{10} dynes/cm^2)	Apparent Strain (ε)
	1	0.00	64.0=R_o^o	0	0
	2	0.1	44.6	-3.06	0.71
	3	0.2	39.0	-4.68	0.99
	4	0.3	36.0	-5.99	1.16
	5	0.4	34.6	-7.33	1.24
LOAD	6	0.5	33.5	-8.64	1.31
	7	0.6	32.6	-9.84	1.35
	8	0.7	32.0	-11.06	1.39
	9	0.8	31.7	-12.40	1.40
	10	0.9	31.5	-13.77	1.42
	11	0.8	31.3	-12.08	1.44
	12	0.7	31.5	-10.68	1.42
	13	0.6	31.5	-9.16	1.42
UNLOAD	14	0.5	31.6	-7.70	1.41
	15	0.4	32.0	-6.32	1.39
	16	0.3	32.4	-4.82	1.36
	17	0.2	33.0	-3.36	1.32
	18	0.1	34.0	-1.78	1.27
	19	0.00	31.3		
	20	-0.05	37.8	+1.05	1.06
	21	-0.10	44.7	+3.08	0.72

TABLE 12

ADHESION RUN C-5, S-8

	No.	Load w (grams)	Contact Resistance R_o (mΩ)	Apparent Stress σ (10^{10} dynes/cm^2)	Apparent Strain (ε)
	1	0.00	$54.2=R_o^o$	0	0
	2	0.1	50.0	-3.73	0.15
	3	0.2	47.0	-6.55	0.28
	4	0.3	44.7	-8.90	0.38
	5	0.4	43.0	-11.00	0.45
	6	0.5	41.8	-12.90	0.51
	7	0.6	39.8	-14.10	0.61
	8	0.7	39.1	-15.85	0.65
LOAD	9	0.8	38.2	-17.20	0.69
	10	0.9	37.7	-19.00	0.72
	11	1.0	37.0	-20.20	0.76
	12	1.1	36.4	-21.60	0.79
	13	1.2	35.8	-22.80	0.82
	14	1.3	35.2	-23.80	0.86
	15	1.4	32.7	-24.80	0.89
	16	1.5	32.8	-25.50	0.94
	17	1.6	33.0	-25.80	0.98
	18	1.5	32.8	-24.00	0.99
	19	1.4	32.7	-22.10	1.00
	20	1.3	32.7	-20.60	1.00
	21	1.2	32.7	-19.00	1.00
	22	1.1	32.8	-17.60	0.99

TABLE 12 (Cont.)

	No.	Load w (grams)	Contact Resistance R_o (mΩ)	Apparent Stress σ (10^{10} dynes/cm^2)	Apparent Strain (ε)
UNLOAD	23	1.0	32.8	-16.10	0.99
	24	0.9	33.0	-14.70	0.98
	25	0.8	33.1	-13.00	0.978
	26	0.7	33.1	-11.40	0.978
	27	0.6	33.3	- 9.90	0.96
	28	0.5	33.8	- 8.52	0.94
	29	0.4	34.3	- 7.00	0.91
	30	0.3	34.7	- 5.37	0.88
	31	0.2	35.2	- 3.68	0.86
	32	0.1	35.8	- 1.90	0.82
	33	0.00	36.4		
	34	-0.1	37.2	+ 2.18	0.68
	35	-0.2	38.5	+ 4.70	0.61
	36	-0.3	39.8	+ 7.35	0.55

TABLE 13

ADHESION RUN C-6, S-13

	No.	Load w (grams)	Contact Resistance R_o (mΩ)	Apparent Stress σ (10^{10} dynes/cm^2)	Apparent Strain (ε)
	1	0.00	$47.5=R_o^o$	0	0
	2	0.1	39.2	-2.27	0.41
	3	0.2	36.8	-4.02	0.53
	4	0.3	35.2	-5.52	0.62
	5	0.4	33.7	-6.73	0.71
	6	0.5	32.7	-7.93	0.77
	7	0.6	32.0	-9.11	0.81
	8	0.7	31.1	-10.00	0.87
	9	0.8	30.8	-11.30	0.89
	10	0.9	30.5	-12.45	0.91
	11	1.0	30.2	-13.55	0.93
	12	1.1	29.8	-14.50	0.95
LOAD	13	1.2	29.5	-15.50	0.97
	14	1.3	29.1	-16.40	1.00
	15	1.4	28.8	-17.25	1.02
	16	1.5	28.3	-17.80	1.05
	17	1.6	27.8	-18.35	1.10
	18	1.7	27.5	-19.05	1.10
	19	1.8	27.3	-19.90	1.13
	20	1.9	27.1	-20.70	1.14
	21	2.0	27.0	-21.65	1.15
	22	1.0	26.7	-20.10	1.17

TABLE 13 (Cont.)

	No.	Load w (grams)	Contact Resistance R_o (mΩ)	Apparent Stress σ (10^{10} dynes/cm^2)	Apparent Strain (ε)
	23	1.8	26.5	-18.80	1.18
	24	1.7	26.5	-17.75	1.18
	25	1.6	26.5	-16.65	1.19
	26	1.5	26.6	-15.70	1.18
	27	1.4	26.6	-14.70	1.18
	28	1.3	26.7	-13.75	1.17
	29	1.2	26.7	-12.75	1.17
	30	1.1	26.7	-11.60	1.17
UNLOAD	31	1.0	26.8	-10.70	1.16
	32	0.9	26.8	-9.60	1.16
	33	0.8	27.0	-8.68	1.15
	34	0.7	27.2	-7.70	1.13
	35	0.6	27.3	-6.77	1.12
	36	0.5	27.5	-5.60	1.11
	37	0.4	27.6	-4.50	1.10
	38	0.3	28.0	-3.53	1.07
	39	0.2	28.4	-2.35	1.05
	40	0.1	29.1	-1.27	1.00
	41	0.00	30.2		
	42	-0.05	30.8	+0.73	0.86
	43	-0.10	31.7	+1.55	0.81

TABLE 14

ADHESION RUN C-7, S-16

	No.	Load w (grams)	Contact Resistance R_o (mΩ)	Apparent Stress σ (10^{10} dynes/cm^2)	Apparent Strain (ε)
	1	0.00	$57.8=R_o^o$	0	0
	2	0.1	52.3	-4.05	0.21
	3	0.2	49.0	-7.12	0.34
	4	0.3	45.5	-9.22	0.49
	5	0.4	42.4	-10.70	0.63
	6	0.5	40.0	-11.87	0.74
	7	0.6	38.3	-13.05	0.83
	8	0.7	36.9	-14.13	0.90
	9	0.8	36.0	-15.40	0.95
	10	0.9	35.3	-16.65	0.99
	11	1.0	34.5	-17.64	1.04
	12	1.1	33.7	-18.60	1.09
	13	1.2	33.0	-19.40	1.13
LOAD	14	1.3	32.2	-20.00	1.18
	15	1.4	31.5	-20.06	1.22
	16	1.5	30.7	-21.00	1.27
	17	1.6	30.0	-21.45	1.32
	18	1.7	29.4	-21.70	1.36
	19	1.8	28.8	-22.20	1.40
	20	1.9	28.1	-22.35	1.45
	21	2.0	27.4	-22.35	1.49
	22	2.1	26.0	-21.15	1.60
	23	2.2	25.0	-20.35	1.68
	24	2.1	25.0	-19.40	1.68
	25	2.0	25.0	-18.55	1.68
	26	1.9	25.0	-17.65	1.68
	27	1.8	25.0	-16.65	1.68
	28	1.7	25.0	-15.70	1.68

TABLE 14 (Cont.)

	No.	Load w (grams)	Contact Resistance R_o (mΩ)	Apparent Stress σ (10^{10} dynes/cm^2)	Apparent Strain (ε)
	29	1.6	25.0	-14.80	1.68
	30	1.5	25.0	-13.95	1.68
UNLOAD	31	1.4	25.0	-13.00	1.68
	32	1.3	25.0	-12.10	1.68
	33	1.2	25.0	-11.10	1.68
	34	1.1	25.0	-10.20	1.68
	35	1.0	25.0	-9.30	1.68
	36	0.9	25.0	-8.35	1.68
	37	0.8	25.0	-7.45	1.68
	38	0.7	25.0	-6.50	1.68
	39	0.6	25.0	-5.60	1.68
	40	0.5	25.0	-4.60	1.68
	41	0.4	25.0	-3.72	1.68
	42	0.3	25.0	-2.78	1.68
	43	0.2	25.1	-1.87	1.67
	44	0.1	25.1	-0.935	1.67
	45	0.00	25.5		
	46	-0.1	25.6	+0.98	1.64
	47	-0.2	25.8	+0.99	1.62
	48	-0.3	26.0	+2.00	1.60
	49	-0.4	26.3	+3.08	1.58
	50	-0.5	26.6	+4.22	1.56
	51	-0.6	27.0	+5.40	1.53
	52	-0.7	27.8	+6.90	1.47
	53	-0.8	29.5	+9.05	1.35
	54	-0.9	33.5	+13.25	1.09
	55	-1.0	43.4	+25.20	0.58

TABLE 15

ADHESION RUN C-8, S-20

	No.	Load w (grams)	Contact Resistance R_o (mΩ)	Apparent Stress σ (10^{10} dynes/cm^2)	Apparent Strain (ε)
	1	0.00	$41.6=R_o^o$	0	0
	2	0.1	32.5	1.57	0.51
	3	0.2	27.7	2.25	0.83
	4	0.3	25.4	2.85	1.00
	5	0.4	23.0	3.14	1.20
	6	0.5	21.5	3.43	1.34
	7	0.6	20.5	3.72	1.43
	8	0.7	19.8	4.06	1.50
	9	0.8	19.0	4.3	1.59
	10	0.9	18.3	4.47	1.66
	11	1.0	18.0	4.81	1.69
	12	1.1	17.7	5.10	1.73
	13	1.2	17.3	5.33	1.77
LOAD	14	1.3	17.1	5.64	1.79
	15	1.4	17.0	6.00	1.81
	16	1.5	16.7	6.21	1.84
	17	1.6	16.5	6.47	1.87
	18	1.7	16.0	6.47	1.93
	19	1.8	15.5	6.41	1.99
	20	1.7	15.6	6.13	1.98

TABLE 15 (Cont.)

	No.	Load w (grams)	Contact Resistance R_o (mΩ)	Apparent Stress σ (10^{10} dynes/cm^2)	Apparent Strain (ε)
	21	1.6	15.7	-5.86	1.97
	22	1.5	15.8	-5.58	1.96
UNLOAD	23	1.4	16.0	-5.32	1.93
	24	1.3	16.1	-5.00	1.91
	25	1.2	16.2	-4.68	1.90
	26	1.1	16.5	-4.45	1.87
	27	1.0	16.8	-4.19	1.83
	28	0.9	17.0	-3.85	1.81
	29	0.8	17.2	-3.52	1.79
	30	0.7	17.4	-3.14	1.76
	31	0.6	17.9	-2.85	1.71
	32	0.5	18.2	-2.46	1.67
	33	0.4	18.8	-2.10	1.61
	34	0.3	19.5	-1.69	1.53
	35	0.2	20.6	-1.27	1.42
	36	0.1	22.2	-0.735	1.28
	37	0.00	24.5		
	38	-0.05	26.2	+0.53	0.93
	39	-0.1	30.2	+1.355	0.66

TABLE 16

ADHESION RUN C-8, S-21

	No.	Load w (grams)	Contact Resistance R_o (mΩ)	Apparent Stress σ (10^{10} dynes/cm^2)	Apparent Strain (ε)
	1	0.00	$46.6=R_o^o$	0	0
	2	0.1	38.4	-2.18	0.40
	3	0.2	34.1	-3.45	0.64
	4	0.3	29.2	-3.80	0.95
	5	0.4	27.0	-4.33	1.11
	6	0.5	26.0	-5.02	1.18
	7	0.6	25.0	-5.57	1.26
	8	0.7	23.8	-5.88	1.36
	9	0.8	23.2	-6.40	1.41
LOAD	10	0.9	22.5	-6.77	1.47
	11	1.0	22.0	-7.2	1.52
	12	1.1	21.9	-7.82	1.53
	13	1.2	21.8	-8.48	1.54
	14	1.3	21.4	-8.82	1.57
	15	1.4	21.1	-9.25	1.60
	16	1.5	20.9	-9.75	1.62
	17	1.4	20.6	-8.81	1.65
	18	1.3	20.7	-8.28	1.64
	19	1.2	20.8	-7.70	1.63
	20	1.1	20.8	-7.08	1.63
UNLOAD	21	1.0	20.9	-6.50	1.62
	22	0.9	21.0	-5.88	1.61
	23	0.8	21.2	-5.33	1.59
	24	0.7	21.4	-4.76	1.57
	25	0.6	21.6	-4.15	1.55
	26	0.5	21.8	-3.53	1.54
	27	0.4	22.0	-2.87	1.52
	28	0.3	22.5	-2.25	1.47
	29	0.2	24.2	-1.74	1.33
	30	0.1	26.0	-1.00	1.18
	31	0.00	31.0	-	-
	32	-0.05	35.6	+0.98	0.54

TABLE 17

ADHESION RUN C-8, S-22

	No.	Load w (grams)	Contact Resistance R_o (mΩ)	Apparent Stress σ (10^{10} dynes/cm^2)	Apparent Strain (ε)
	1	0.00	$39.3=R_o^o$	0	0
	2	0.1	29.0	-1.25	0.59
	3	0.2	25.4	-1.92	0.86
	4	0.3	22.4	-2.24	1.11
	5	0.4	20.8	-2.57	1.26
	6	0.5	19.8	-2.92	1.36
	7	0.6	18.8	-3.14	1.46
	8	0.7	18.1	-3.40	1.54
	9	0.8	17.8	-3.75	1.57
	10	0.9	17.5	-4.10	1.60
	11	1.0	16.8	-4.20	1.68
	12	1.1	16.4	-4.39	1.73
	13	1.2	16.1	-4.62	1.77
LOAD	14	1.3	15.8	-4.82	1.81
	15	1.4	15.5	-5.00	1.85
	16	1.5	15.3	-5.21	1.87
	17	1.6	15.1	-5.42	1.90
	18	1.7	15.1	-5.75	1.90
	19	1.8	15.0	-6.02	1.91
	20	1.9	14.7	-6.10	1.95
	21	2.0	14.5	-6.25	1.98
	22	2.1	14.2	-6.30	2.02

TABLE 17 (Cont.)

	No.	Load w (grams)	Contact Resistance R_o (mΩ)	Apparent Stress σ (10^{10} dynes/cm^2)	Apparent Strain (ε)
	23	2.0	14.5	-6.25	1.98
	24	1.9	14.6	-6.02	1.97
	25	1.8	14.7	-5.79	1.95
UNLOAD	26	1.7	14.8	-5.53	1.94
	27	1.6	14.9	-5.27	1.92
	28	1.5	14.9	-4.95	1.92
	29	1.4	15.0	-4.68	1.91
	30	1.3	15.2	-4.45	1.88
	31	1.2	15.5	-4.28	1.85
	32	1.1	15.6	-3.98	1.83
	33	1.0	15.8	-3.70	1.81
	34	0.9	16.0	-3.42	1.78
	35	0.8	16.5	-3.24	1.72
	36	0.7	16.7	-2.90	1.70
	37	0.6	17.0	-2.58	1.66
	38	0.5	17.8	-2.35	1.57
	39	0.4	18.2	-1.96	1.52
	40	0.3	19.0	-1.61	1.44
	41	0.2	20.1	-1.20	1.33
	42	0.1	21.1	-0.66	1.23
	43	0.00	25.3	-	-

APPENDIX III

COEFFICIENT OF DYNAMIC FRICTION FOR COBALT-50 IRON AND COBALT-25 MOLYBDENUM-10 CHROMIUM ALLOYS

TABLE 18

PREDICTED COEFFICIENT OF DYNAMIC FRICTION FOR THE Co-50Fe SYSTEM AT VARIOUS CLEANING CONDITIONS, TAKEN AT A CONTACT OPERATIONAL STRESS LEVEL OF 71,100 P.S.I. FOR THE CROSSED WIRE CONFIGURATION

Condition	ε (Strain)	μ (for α=11 and 3)
Thermal Degas (Figure 16)	1.00	0.74 to 1.42
Thermal Degas (Figure 17)	1.41	1.16 to 2.22
Code C-1, Serial No. 1	1.21	0.95 to 1.81
Code C-5, Serial No. 8	0.78	0.57 to 1.10
Code C-6, Serial No. 13	0.95	0.72 to 1.35
Code C-7, Serial No. 16	1.66	1.54 to 2.94
Code C-8, Serial No. 20	1.31	0.99 to 1.89
Code C-8, Serial No. 21	1.12	0.80 to 1.53
Code C-8, Serial No. 22	1.27	0.96 to 1.83

The Co-25Mo-10Cr System, Ultra High Clean Surface

Condition	ε (Strain)	μ (for α=11 and 3)
Ultra Clean Surface	0.32	0.29 to 0.55

BIBLIOGRAPHY

1. Keller, D.V., "Adhesion or Cold Welding of Materials in Space Environments," ASTM-STP, 431 (1968), p. 5 and p. 181.

2. Merchant, M.E., "Friction and Adhesion," NASA Symposium, San Antonio, Texas (1967), 4.7.

3. Tabor, D., "Friction and Adhesion," NASA Symposium, San Antonio, Texas (1967), 7.4.

4. Williamson, J.B.P., "Topography of Solid Surface," NASA Symposium, San Antonio, Texas, (1967), 2.3.

5. Keller, D.V., Discussion of the Paper, "Friction and Adhesion," by M.E. Merchant, NASA Symposium, San Antonio, Texas (1967), 4.7.

6. Keller, D.V. and Johnson, K.I., "Effect of Contamination on the Adhesion of Metallic Couples in Ultra High Vacuum," J. of Applied Physics, vol. 38, no. 4, 1896-1902, 15 March (1967).

7. Greenwood, J.A., et al., "Contact of Nominally Flat Surfaces," Proc. Roy. Soc. A 295, 300 (1966).

8. Buckley, D.H., "The Influence of Crystal Structure, Orientation and Solubility on the Adhesion and Sliding of Various Metal Single Crystals in Vacua," ASTM-STP, 431, (1968), p. 248.

9. Buckley, D.H., "Influence of Crystal Structure on Friction Characteristics of Rare Earth and Related Metals in Vacuum to 10^{-10} Torr," NASA Report TND-2513 (1964).

10. Conrad, H., and Rice, L., "Cold Welding of Copper Under Ultra High Vacuum," ASTM-STP (1968), p. 216.

11. Gilbreath, W.P., "Definition and Evaluation of Parameters Which Influence the Adhesion of Metals," ASTM-STP, 431, (1968), p. 128.

12. Muller, E.W., and Nishikawa, O., "Atomic Surface Structure of the Common Transition Metals and the Effect of Adhesion As Seen by Field Ion Microscopy," ASTM-STP, 431, (1968), p. 67.

13. Keller, D.V., and McNicholas, T., "Utilization of Contact Resistance Measurements in the Investigation of the Metallic Adhesion of Iron," J. of Adhesion, vol. 1, July 1969.

14. Tsai, M.H., "Investigation of the Effect of Adsorbed Hydrogen on the Adhesion of Ultra Clean Iron - 8 ppm Carbon Couples Using Contact Resistance Techniques," Master's Thesis (1969), Syracuse University, Syracuse, N. Y.

15. Keller, D.V., and Aldrich, R.G., "Adhesion of Metallic Bodies Initiated by Physical Contact," J. of Adhesion, vol. 1, April 1969.

16. Milner, D.R., and McIntyre, D.V., Metallurgical Reviews, 7, 433, (1962).

17. Keller, D.V., "Status and Significance of Metallic Adhesion Research," Presented at Amer. Vac. Soc., N.Y., June 1967.

18. Davison, C. st. C., "Wear Prevention in Early History," 'Wear', vol. 1, 1957, p. 155.

19. Amontons, G., "De la Resistance Causee dans le Machines Mathe matique et Physique," Momoires de l'academie, Royale de Science, 1699, p. 206. As noted in reference 34, p. 503.

20. Coulomb, C.A., "Theorie des Machines Simples," Memoire de Mathematique et de Physique de l'academie Royale, 1785, p. 161.

21. DeSaguliers, J.T., "Some Experiments Concerning the Cohesion of Lead," Phil. Trans. Roy. Soc., vol. 33, no. 389, 1724, p. 335. As noted in reference 34, p. 508.

22. Vince, S., "On the Motion of Bodies Affected by Friction," Phil. Trans. Roy. Soc., vol. 75, 1785, p. 654. As noted in reference 34, p. 509.

23. Leslie, J., "An Experimental Enquiry into the Nature and Propagation of Heat," J. Mawman, London, 1804. As noted in reference 34, p. 510.

24. Bowden, F.P., and Tabor, D., "The Friction and Lubrication of Solids," Part II, Clarendon Press, Oxford, 1964, p. 511.

25. Ewing, Sir A., "The Inner Structure of Simple Metals," Not. Proc. Roy. Instn., vol. 13, 1892, p. 387. As noted in reference 34, p. 511.

26. Hardy, W.B., "Problems of the Boundary State," Phil. Trans. Roy. Soc., vol. A 230, (1931), p. 1.

27. Tomlinson, G.A., "A Molecular Theory of Friction," Phil. Mag., vol. 7, Suppl. June 1929, p. 905.

28. Bowden, F.P., and Tabor, D., "The Friction and Lubrication of Solids," Clarendon Press, Oxford, (1954).

29. Bowden, F.P., and Tabor, D., "The Friction and Lubrication of Solids," Part II, Clarendon Press, Oxford, (1964).

30. Braithwaite, E.R., "Solid Lubricants and Surfaces," Pergamon Press, Oxford, (1964), p. 2-5.

31. Holm, R., "Electric Contacts," Springer-Verlag Inc., N.Y., 4th edition, (1967), p. 103.

32. Greenwood, J.A., "Constriction Resistance and Real Area of Contact," Brit. J. Appl. Phy. 17, 1621 (1966).

33. Tabor, D., "The Hardness of Metals," Oxford, England (1954).

34. Ellis, W.C., and Greiner, E.S., "Equilibrium Relations in the Solid State of the Iron-Cobalt System," Transactions of ASM 29, 415-432, (1941).

35. Hansen, M., "Constitution of Binary Alloys," 2nd edition, McGraw Hill Book Co., N.Y. (1958).

36. Pearson, W.B., "A Handbook of Lattice Spacings and Structures of Metals and Alloys," Pergamon, N.Y. (1958).

37. Cullity, B.D., "Elements of X-Ray Diffraction," Addison-Wesley Publishing Co., Inc., (1967).

38. Rideout, S.P., and Beck, P.A., "Survey of Portions of the Chromium-Cobalt-Nickel-Molybdenum Quaternary System at 1200°C," Report 1122, NACA, which supercedes NACA TN 2683, "Survey of Portions of Chromium-Cobalt-Nickel-Molybdenum Quaternary System at 1200°C, by Rideout, S.P., and Beck, P.A., (1952).

39. Lux, B., and Bollmann, W., "Precipitation Hardening of Cobalt Base Alloys By Means of an Intermetallic Cobalt-Molybdenum Phase," Cobalt 11, June (1961).

40. Alte da Beiga, L., ACTA Cryst, 18, 857, (1965).

41. McNicholas, T., "Investigation of the Adhesion Between Ultra-Clean Iron-65 p.p.m. Carbon Couples Utilizing Contact Resistance Techniques," Master's Thesis (1968), Syracuse University, Syracuse, N.Y.

42. Richardson, F.D., and Jeffes, J.H.E., J. Iron and Steel Inst., 160, 3261, (1948).

43. McFarlane, J.S., and Tabor, D., Proc. Roy. Soc., 202A, 244, (1950).

44. Keller, D.V., and Tsai, M., NASA Report, "Adhesion Between Atomically Pure Metal Surfaces," July, (1969), Met. 1100-0769-F. Reported to Physics of Adhesion Conference, Karlsrhue, Germany, (1969).

45. Roark, R.J., "Formulae for Stress and Strain," 1965, 4th edition, McGraw Hill.

46. Buckley, D.H., and Johnson, R.L., "Influence of Crystal Structure and Some Properties of Hexagonal Metals on Friction and Adhesion," Wear, vol. 11, 1968, pp. 405-419.

47. Kragelskii, I.V., "Friction and Wear," Butterworths, Washington, (1965).

48. Brainard, W.A., and Buckley, D.H., "Effect of Crystal Transformation and Atomic Ordering on Friction and Wear of Two Cobalt Base Alloys in Vacuum," NASA TN D-4668, 1968.

49. Farnsworth, H.E., Schlier, R.E., George, T.H., and Burger, R.M., J. App. Phy., 29, 8, (1958).

50. Farnsworth, H.E., "The Solid-Gas Interface," Ed. Flood, E.A., Dekker, (1967).

51. Kaminsky, M., "Atomic and Ionic Impact Phenomena on Metal Surfaces," Springer-Verlag, (1965).

52. Asada, T., and Quasebarth, K., "The Extraction of Gold From Cathode Metal By Glow Discharge," Z. Physik. Chem., A143, 435, (1929).

53. Ogilvie, G.J., and Ridge, M.J., "Bombardment of Metals by Inert Gas Ions," Aust. J. Phy. 13, 402, (1960).

54. Fisher, T.F., and Weber,C.E., "Cathode Sputtering for Micro-Diffusion Studies," J. App. Phy., 23, 181, (1952).

55. Hanau, R., "Cathode Sputtering in the Abnormal Glow Discharge," Phys. Rev., 76, 153 (1949).

56. Singleton, J.H., J. Vac. Sci. and Tech., 3, 354, (1966).

57. Buckley, D.H., "Influence of Chemisorbed Films on the Adhesion and Friction of Clean Iron," NASA TND 4775, (1958).

58. Hume-Rothery, W., "The Engel-Brewer Theories of Metals and Alloys," Prog. in Materials Science, vol. 13, no. 5, (1967).

59. Goodenough, J.B., "Magnetism and the Chemical Bond," Interscience Publishers, (1963).

60. Archard, J.F., "Contact and Rubbing of Flat Surfaces," J. App. Phy., 24, (1953), 981-983.

NASA-Langley, 1972 — 15 E-6655